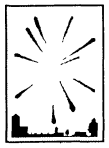

Meteoritics & Planetary Science 36, 761–781 (2001)
Available online at http://www.uark.edu/meteor

Vesta, Vestoids, and the howardite, eucrite, diogenite group: Relationships and the origin of spectral differences

T. H. BURBINE[1]*, P. C. BUCHANAN[2]†, R. P. BINZEL[3], S. J. BUS[3]‡, T. HIROI[4], J. L. HINRICHS[5], A. MEIBOM[5]§ AND T. J. McCOY[1]

[1]Department of Mineral Sciences, National Museum of Natural History, Smithsonian Institution, Washington, D.C., 20560-0119, USA
[2]NASA Johnson Space Center, Mail Code SN2, Houston, Texas 77058, USA
[3]Department of Earth, Atmospheric, and Planetary Sciences, Massachusetts Institute of Technology, Cambridge Massachusetts 02139, USA
[4]Department of Geological Sciences, Brown University, Providence, Rhode Island 02912, USA
[5]Hawai'i Institute of Geophysics and Planetology, University of Hawai'i at Manoa, Honolulu, Hawai'i 96822, USA
†Present address: Department of Geology, University of the Witwatersrand, Private Bag 3, Wits 2050, Johannesburg, South Africa
‡Present address: Institute for Astronomy, 640 North A'ohoku Place, Hilo, Hawai'i 96720, USA
§Present address: Department of Geological and Environmental Sciences, Stanford University, Building 320, Lomita Mall, Stanford, California 94305, USA
*Correspondence author's email address: burbine.tom@nmnh.si.edu

(Received 2000 May 18; accepted in revised form 2001 February 16)

Abstract–Spectra of asteroid 4 Vesta and 21 small (estimated diameters less than 10 km) asteroids with Vesta-like spectral properties (Vestoids) were measured at visible and near-infrared wavelengths (~0.44 to ~1.65 μm). All of the measured small asteroids (except for 2579 Spartacus) have reflectance spectra consistent with surface compositions similar to eucrites and howardites and consistent with all being derived from Vesta. None of the observed asteroids have spectra similar to diogenites. We find no spectral distinction between the 15 objects tabulated as members of the Vesta dynamical family and 6 of the 7 sampled "non-family" members that reside just outside the semi-major axis (a), eccentricity (e), and inclination (i) region of the family. The spectral consistency and close orbital (a-e-i) match of these "non-family" objects to Vesta and the Vesta family imply that the true bounds of the family extend beyond the subjective cut-off for membership. Asteroid 2579 Spartacus has a spectrum consistent with a mixture of eucritic material and olivine. Spartacus could contain olivine-rich material from Vesta's mantle or may be unrelated to Vesta altogether. Laboratory measurements of the spectra of eucrites show that samples having nearly identical compositions can display a wide range of spectral slopes. Finer particle sizes lead to an increase in the slope, which is usually referred to as reddening. This range of spectral variation for the best-known meteoritic analogs to the Vestoids, regardless of whether they are actually related to each other, suggests that the extremely red spectral slopes for some Vestoids can be explained by very fine-grained eucritic material on their surfaces.

INTRODUCTION

The howardite, eucrite, and diogenite (HED) meteorites form a related series of igneous/volcanic rocks distinguished by continuous variations in mineralogy and chemistry (*e.g.*, Mason, 1962; Dodd, 1981; Mittlefehldt *et al.*, 1998). These meteorites are believed to have formed on the same parent body or related parent bodies. This suite of meteorites includes basalts of both intrusive and extrusive origin (eucrites), intrusive orthopyroxenites (diogenites), monomict and polymict breccias containing only eucritic or diogenitic material, and polymict breccias containing both lithologic units (howardites). Mineralogically, eucrites contain primarily anorthitic plagioclase and low-Ca pyroxene with augite exsolution lamellae, while diogenites are predominately magnesian orthopyroxene.

Asteroid 4 Vesta has been postulated (*e.g.*, McCord *et al.*, 1970; Larson and Fink, 1975; Consolmagno and Drake, 1977) as the parent body of the HED meteorites due to Vesta's distinctive reflectance spectrum, which is similar in structure to the laboratory spectra of HED meteorites. Recent reviews (Drake, 2001; Binzel, 2001) of the current evidence strongly endorse this link. Both Vesta and the HED meteorites have two spectral features centered near 0.9–1 μm (Band I) and 1.9–2 μm (Band II). The positions of these features are a function of pyroxene composition (Adams, 1974) with eucrites having band minima that are shifted to longer wavelengths than the diogenites due to the more Ca- and Fe-rich nature of their

Prelude preprint MS4373

pyroxenes (Gaffey, 1976). The positions of Vesta's absorption bands appear to be best matched by some combination of eucritic and diogenitic material (possibly analogous to a howardite) (Hiroi *et al.*, 1994; Gaffey, 1997).

Vesta, with a mean diameter of 506 km (Thomas *et al.*, 1997a), is the only object with a diameter greater than 50 km with this distinctive spectrum. Vesta is also the largest body in a dynamical family of asteroids (Fig. 1) (*e.g.*, Williams, 1979; Zappalà *et al.*, 1990, 1995), which share similar proper orbital elements (where the effects of planetary perturbations have been removed). Zappalà *et al.* (1995) included over 200 members in their Vesta family. They used two clustering techniques, the hierarchical clustering method (HCM) and the wavelet analysis method (WAM), with the size and membership of the family depending on the clustering algorithm. These methods are used to find statistically significant clusters of objects. The presently defined HCM Vesta family region, including tentative members, extends from ~2.26 to ~2.47 AU, ~0.08 to ~0.12 in proper eccentricity, and ~0.10 to ~0.14 in proper sine of inclination. Tentative members are found at a slightly higher distance level than "nominal" family members. The "nominal" HCM Vesta family is generally thought to be too conservative (*e.g.*, Marzari *et al.*, 1996) in which objects it includes as members.

Binzel and Xu (1993) identified a number of small asteroids with "Vesta-like" visible spectra (usually called Vestoids). All of these "Vesta-like" objects were found in the Vesta family and between Vesta and meteorite-supplying resonances such as the 3:1 (~2.5 AU) and υ_6 (Fig. 1), supporting the argument that HED meteorites are fragments of Vesta. However, the Vestoids are not perfect spectral matches for Vesta and tend to have higher reflectance values with increasing wavelength for spectra normalized to unity at 0.55 μm (*e.g.*, Hiroi and Pieters, 1998). The asteroids with the strongest ultraviolet (UV) features and deepest 1 μm bands were interpreted as having compositions similar to diogenites. Binzel and Xu (1993) proposed the J class for these objects, which is mnemonic for the diogenite Johnstown.

Objections have been raised to linking Vesta with the Vestoids. Wasson *et al.* (1996) suggested that fragments of a projectile that had a grazing impact with Vesta are coated with "Vesta dust" and, thus, appear "Vesta-like". Bell (1998) proposed that most Vestoids are background S asteroids with deeper 1 μm bands since observations of the Vestoids (Burbine and Binzel, 1997; Burbine *et al.*, 1998) showed that their spectra had greater continuum slopes than Vesta. Vilas *et al.* (2000) found that some Vestoids lack an ~0.5065 μm absorption feature that is present in all spectra of Vesta by Cochran and Vilas, 1998. This absorption band is a spin-forbidden Fe^{2+} feature in sixfold coordination, whose structure and shape is correlated with the amount and form of calcium in pyroxenes (Hazen *et al.*, 1978).

In this paper, we examine the spectral similarities and differences between Vestoids and Vesta and examine the HED suite of meteorites in an effort to understand the nature of these

TABLE 1. Asteroids in the HCM Vesta family, including tentative members, that have been observed in SMASSIR.

Asteroid	Proper elements*			Diameter† (km)	Family‡		SMASS§	
	a' (AU)	e'	sin i'		HCM	WAM	I	II
4 Vesta	2.362	0.099	0.111	506	Vesta	Vesta	V	V
1906 Naef	2.374	0.100	0.112	6	Vesta	Vesta	V	–
1929 Kollaa	2.363	0.114	0.123	8	Vesta	Vesta	V	V
1933 Tinchen	2.353	0.094	0.119	5	Vesta	Vesta	V	–
2045 Peking	2.380	0.090	0.116	8	Vesta	Vesta	–	V
2590 Mourào	2.343	0.097	0.117	6	Vesta	Vesta	V	–
3268 De Sanctis	2.347	0.100	0.122	4	Vesta	Vesta	V	–
3376 Armandhammer	2.349	0.097	0.123	9	Vesta	Vesta	–	Sq
3657 Ermolova	2.313	0.085	0.115	6	Vesta		J	–
3944 Halliday	2.368	0.109	0.118	5	Vesta	Vesta	V	–
3968 Koptelov	2.322	0.091	0.116	5	Vesta	Vesta	V	–
4005 Dyagilev	2.452	0.113	0.105	6	Vesta		J	–
4147 Lennon	2.362	0.102	0.113	5	Vesta	Vesta	V	–
4215 Kamo	2.417	0.098	0.115	7	Vesta		J	V
4900 Maymelou	2.379	0.102	0.114	5	Vesta	Vesta	–	V

*Proper elements (a', e', sin i') are from Milani and Knežević (1994).
†Vesta's diameter is from Thomas *et al.* (1997a). The rest of the diameters are calculated using the absolute magnitude with an estimated albedo of 0.42 (Vesta's Infrared Astronomical Satellite (IRAS) albedo). The diameter is estimated to be equal to $10^{((6.259-0.4H-\log p)/2)}$ (Bowell *et al.*, 1989) where H is the absolute magnitude (the time-averaged magnitude of an asteroid calculated at zero phase angle and unit heliocentric and geocentric distances) and p is the visual albedo. Lowering the estimated albedos of the Vestoids to 0.25 raises the estimated diameters by ~2 km.
‡Family memberships are from Zappalà *et al.* (1995).
§SMASS I classifications are from Xu *et al.* (1995) and SMASS II are from Bus (1999, pers. comm.).

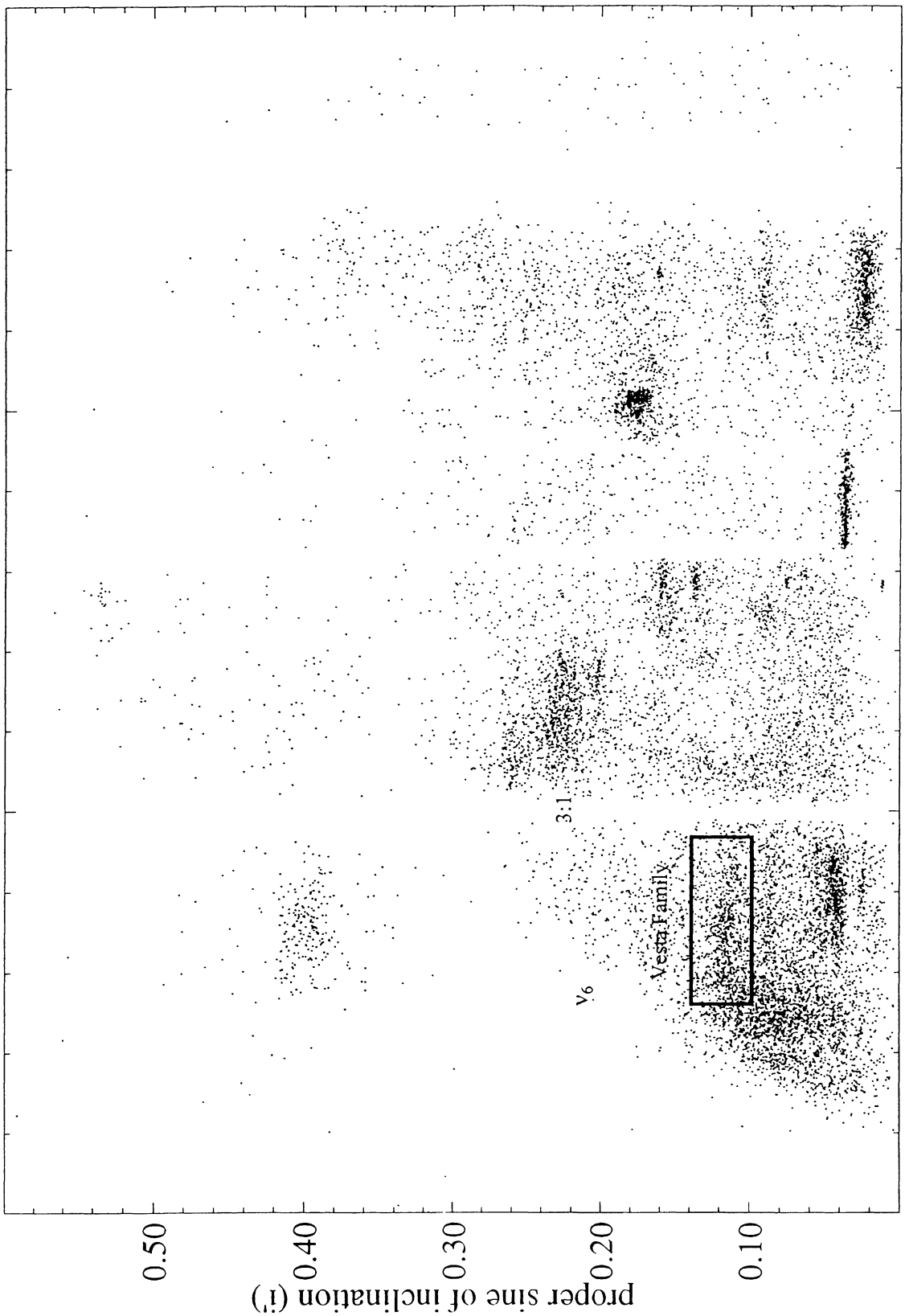

FIG. 1. Plot of proper semi-major axis (a') (in AU) *vs.* proper sine of inclination (i') for main belt asteroids. Proper elements for low-inclination objects are from Milani and Knežević (1994) and high-inclination objects are from LeMaitre (pers. comm.). A box outlines (approximately) the Vesta family region, including tentative members, defined by the hierarchical clustering method (HCM). Approximate locations of the 3:1 and ν_6 (arcing gap that bounds the inner main belt) resonances are also labeled.

differences. We have observed 15 asteroids (including Vesta) in the HCM Vesta family (Table 1) in the near-infrared out to 1.65 μm. These objects are compared to seven Vestoids in the inner main belt that fall outside the HCM Vesta family (Table 2). We have also studied HED meteorites, the closest meteorite analogs to Vesta. Reflectance spectra have been measured for several eucrite and howardite samples to examine the effects of varying mineralogy, mineral and bulk compositions, grain size, and temperature on spectral properties. All of these observations should provide insight into whether Vestoids are fragments of Vesta.

OBSERVATIONAL TECHNIQUES

The visible charge-coupled device (CCD) asteroid spectra were taken at the 1.3 and 2.4 m telescopes at the Michigan-Dartmouth-MIT (MDM) observatory at Kitt Peak in Arizona as part of the Small Main-Belt Asteroid Spectroscopic Survey (SMASS). Data acquisition procedures and data reduction techniques for SMASS are described in Xu *et al.* (1995) (SMASS I) and Bus (1999) (SMASS II). SMASS I spectrally observed over 300 asteroids, mainly in the inner main belt, using a CCD with usable wavelength coverage ~0.48 to ~1.0 μm. SMASS I observations have no plotted error bars, but have estimated overall uncertainties typically in the range of 1 to 2%. The SMASS I spectra have a dispersion of 0.001 μm per pixel (10 Å per pixel) for a resolution of 0.002 μm (2 pixel).

SMASS II observed over 1400 asteroids with most of these objects listed in Bus (1999). A slightly different CCD from SMASS I was used. The SMASS II CCD was more responsive at shorter wavelengths, but less at longer wavelengths. The usable wavelength coverage of SMASS II is from ~0.44 to ~0.92 μm. The data cut off at the telluric water band, which is centered at ~0.94 μm. However, the SMASS I spectra past ~0.92 μm may also be affected by the same atmospheric absorption feature. SMASS II data have 1σ error bars for individual points. The SMASS II spectra have a dispersion of 0.0025 μm per pixel (25 Å per pixel) for a resolution of 0.005 μm (2 pixel).

The near-infrared CCD spectra were taken as part of the small main belt asteroid survey in the near-infrared (SMASSIR) (Burbine, 2000) at the NASA Infrared Telescope Facility (IRTF), which is located at Mauna Kea on the island of Hawai'i. A low-resolution "asteroid" grism with appropriate blocking filters designed by Richard Binzel is used to record a simultaneous first-order spectrum from ~0.90 to ~1.65 μm on the NSFCAM (National Science Foundation camera) InSb array. The dispersion is 0.013 μm per pixel (130 Å per pixel) for a resolution of 0.026 μm (2 pixel). The wavelength calibration was obtained by taking spectral images of the flatly-illuminated dome through a number of narrow band filters. The SMASSIR wavelengths overlap the visible CCD coverage of SMASS. Spectral coverage past ~1.65 μm is not possible due to the overlap of a second-order spectrum.

Observational parameters for the SMASSIR observations of the objects plotted in this paper are given in Table 3. Each asteroid spectrum is divided by a standard (solar analog) star observed at a similar airmass and time to produce the reflectance spectrum for each asteroid relative to the Sun. Each asteroid spectrum was taken in a similar fashion except for 4 Vesta. Due to Vesta's brightness, its spectrum was taken from a defocused image and divided by the spectrum of a defocused standard star.

Multiple images are taken for each asteroid and standard star. Images are obtained in pairs (images "A" and "B") where the spectra fall on alternating parts of the CCD chip. As much as possible, the "A" image is repeatedly placed on the same column (and similarly for the "B" image). Image "A" is

TABLE 2. Inner Main Belt Vestoids (not in the HCM Vesta family) observed in SMASSIR.

Asteroid	Proper elements*			Diameter† (km)	SMASS‡	
	a' (AU)	e'	sin i'		I	II
1273 Anchises	2.394	0.123	0.109	6	V	–
2442 Corbett	2.388	0.097	0.095	6	J	–
2579 Spartacus	2.210	0.081	0.103	5	–	V
2653 Principia	2.444	0.115	0.089	8	–	V
2763 Jeans	2.404	0.179	0.075	8	–	V
2851 Harbin	2.478	0.120	0.136	7	–	V
4188 Shulnazaria	2.335	0.112	0.098	6	–	V

*Proper elements (a', e', sin i') are from Milani and Knezevic (1994).

†Diameters are calculated using the absolute magnitude with estimated albedos of 0.42 (Vesta's IRAS albedo). The diameter is estimated to be equal to $10^{((6.259-0.4H-\log p)/2)}$ (Bowell *et al.*, 1989) where H is the absolute magnitude (the time-averaged magnitude of an asteroid calculated at zero phase angle and unit heliocentric and geocentric distances) and p is the visual albedo. Lowering the estimated albedos of the Vestoids to 0.25 raises the estimated diameters by ~2 km.

‡SMASS I classifications are from Xu *et al.* (1995) and SMASS II are from Bus (1999).

TABLE 3. Observational parameters for the SMASSIR objects.

Asteroid	Date*	Time (U.T.)*	Airmass†	Images‡	Standard star§	Airmass†
4 Vesta	30/01/97	14:17–14:25	1.35	7	Hyades 64	1.03
1273 Helma	30/04/98	10:50–11:17	1.44	14	102-1081	1.11
1906 Naef	17/09/98	14:51–15:23	1.02	12	Hyades 64	1.04
1929 Kollaa	08/02/97	07:45–08:36	1.05	20	Hyades 64	1.01
1933 Tinchen	02/05/98	08:57–09:26	1.06	14	102-1081	1.08
2045 Peking	27/02/99	08:43–09:25	1.01	20	102-1081	1.08
2442 Corbett	16/09/98	06:20–06:42	1.21	10	112-1333	1.07
2579 Spartacus	02/10/97	12:51–13:19	1.13	14	93-101	1.07
2590 Mourào	09/02/97	08:16–08:35	1.08	10	Hyades 64	1.01
2653 Principia	15/09/98	11:40–12:13	1.10	16	112-1333	1.06
2763 Jeans	27/01/99	11:37–12:20	1.04	14	Hyades 64	1.12
2851 Harbin	01/03/99	09:21–09:39	1.05	10	Hyades 64	1.06
3268 De Sanctis	01/10/97	12:17–12:57	1.06	13	Hyades 64	1.00
3376 Armandhammer	04/01/98	11:26–11:54	1.09	14	Hyades 64	1.04
3657 Ermolova	09/02/97	07:05–07:23	1.02	12	Hyades 64	1.01
3944 Halliday	02/05/98	11:11–11:44	1.22	16	102-1081	1.08
3968 Koptelov	29/04/98	08:33–09:11	1.30	20	102-1081	1.07
4005 Dyagilev	08/02/97	10:43–11:31	1.02	20	Hyades 64	1.01
4147 Lennon	29/04/98	07:24–08:08	1.14	18	102-1081	1.07
4188 Kitezh	15/09/98	14:40–15:00	1.01	6	Hyades 64	1.01
4215 Kamo	15/09/98	10:28–11:00	1.03	16	112-1333	1.06
4900 Maymelou	23/05/99	13:28–14:01	1.24	14	102-1081	1.18

*Dates (day/month/year) and times of the observations are in universal time (U.T.).
†The quoted airmass is the average airmass for the set of observations.
‡The number of images is the number of exposures that were used in the reduction of the asteroid spectrum.
§Standard stars that have numbers for names are from the Landolt (1973) listing of UBV (ultraviolet, blue, visible) standard stars.

subtracted by "B" and *vice versa* to remove background counts from the sky in each image. Spectral data reduction was done using the image reduction and analysis facility (IRAF), developed by the National Optical Astronomical Observatories (NOAO). The IRAF package *apall* was used to produce a spectrum from each image by summing the pixel values within a specified aperture at each point along the dispersion axis and subtracting any remaining background level.

Since the different parts of the CCD chip may have different sensitivities, spectra from each image from the "A" side of the chip are combined to produce a composite "A" spectrum for a particular object, and similarly for the "B" side spectra. The composite asteroid spectrum from the "A" side is divided by the spectrum of the composite standard star from the "A" side, and similarly for the "B" side spectra. The "A" and "B" reflectance spectra are combined to produce the final reflectance spectrum for a particular night.

An atmospheric water band centered at ~1.4 μm causes the points between 1.35 and 1.5 μm to be very suspect and not usable for most asteroids. Due to the problems in correcting for atmospheric water, no corrections have been made and points that appear to have been affected significantly have been deleted. Weaker atmospheric effects are also sometimes present in the spectra at ~0.94 and ~1.15 μm. The average uncertainty in the spectral slope for an asteroid spectrum at the SMASSIR wavelengths is on the order of 5%, which is comparable to slope uncertainties in the visible (Bus, 1999). For objects (1929 Kollaa and 4005 Dyagilev) observed twice, only the spectra with the lowest residual atmospheric water features are plotted.

One sigma error bars for the reflectance values were calculated using Poisson statistics. The signal-to-noise ratio for each image was calculated by dividing the signal (the summed pixel values with the remaining background level removed from the subtracted images) by the noise (the square root of the summed pixel values with no remaining background level removed from the unsubtracted images). The inverse of the signal-to-noise is the fractional error for each image. The fractional errors for each standard star and asteroid image could be propagated to produce the 1σ error bars for the final composite spectra.

Each SMASSIR spectrum was normalized to a visible spectrum. The normalization to the visible spectrum was done by first fitting the SMASSIR spectrum with errors using a cubic spline program (Reinsch, 1967) that was adapted by Schleicher (pers. comm.) and has been previously used by Bus (1999). Points that appeared significantly affected by atmospheric water features were not used. The SMASSIR spectra were fit from 0.92 to 1.65 μm at 0.01 μm intervals. The 0.92 μm endpoint

was chosen since the SMASS II spectra were fit from 0.44 to 0.92 μm (Bus, 1999) and the two fits could be directly overlapped. Also, the number of counts measured shortward of 0.92 μm in SMASSIR is rapidly decreasing, which increases the uncertainty in the value of those points. The SMASS I data were also fit from 0.44 to 0.92 μm. The SMASSIR fit was then normalized to the fitted visible spectrum. The actual SMASSIR spectrum was multiplied by this normalization factor and then overlaid on the visible spectrum to get the best continuous spectrum from ~0.44 to ~1.65 μm. The final composite spectra of Vesta and the Vestoids are plotted individually in Fig. 2.

Vestoids

Vesta and 14 Vestoids in the HCM Vesta family were observed in SMASSIR (Fig. 3). The observed Vestoids have estimated diameters less than 10 km and were classified as V or J objects except for one deep-featured S-type (3376 Armandhammer) (Bus, 1999). Also plotted are spectra of the eucrite Juvinas, the howardite Le Teilleul, and the diogenite Johnstown (Gaffey, 1976). All spectra of Gaffey (1976) in this paper have had a correction factor of +0.025 μm added to the original wavelengths to compensate for a later-discovered calibration offset (Gaffey, 1984). The correction does not appear to be entirely linear over the entire wavelength range since the ~0.5065 μm feature appears offset by ~0.015 μm in the Gaffey (1976) HED spectra compared to newly measured HED spectra.

These objects have the distinctive 1 μm feature due to pyroxene plus the start of the 2 μm feature. These absorption bands are similar to those found in eucrites and howardites (Fig. 3). The observed objects have spectra redder (higher reflectances at wavelengths longward of 1 μm) than Vesta and some are redder than the reddest eucrite spectrum (Juvinas) from Gaffey (1976). The widths of the 1 μm bands are narrower than the widths found in HED spectra. Except for 4 Vesta and 4215 Kamo (the least red-sloped objects), these objects have a very continuous range of spectral properties. Many of the Vestoids appear (Fig. 2) to have possible features at ~0.5065 μm; however, our lower spectral resolution compared to the Vilas *et al.* (2000) data and scatter in our asteroid spectra makes interpreting the presence of this feature difficult.

These asteroids have band minima between 0.91 and 0.93 μm (error bars of $\pm$0.02 μm), which are consistent with the minima for HED meteorites (0.92 to 0.94 μm). These objects bear more resemblance to eucrites and howardites than diogenites. Eucrites and howardites have turnovers between the 1 and 2 μm features at much higher wavelengths (by at least 0.1 μm) than the turnover in diogenite spectra (Fig. 3). It is difficult to differentiate between eucrites and howardites on the basis of band positions from SMASS and SMASSIR spectra due to a number of factors. First, the differences in 1 μm band minima are very slight between eucrites and howardites. Second, the water feature at ~1.4 μm makes a very accurate determination of the exact turnover between the 1 and 2 μm features difficult. Third, there is no spectral coverage of the 2 μm band minimum, which is more diagnostic in differentiating between these two assemblages.

The asteroids classified as J objects by Binzel and Xu (1993) and observed in SMASSIR are plotted in Fig. 4. These objects all have turnovers between the 1 and 2 μm features at similar wavelengths to those found in eucrites and howardites. These asteroids all have spectra that bear more resemblance to eucrites and howardites than diogenites.

Seven inner main belt Vestoids not in the Vesta family were observed in SMASSIR (Fig. 5). These objects are all located relatively near the Vesta family region, but fall out of the "defined" Vesta family in at least one of the proper elements. Except for 2579 Spartacus, their spectra are indistinguishable from the spectra of Vesta family members as they all show similar pyroxene absorption features. Spartacus (Figs. 2 and 5) has a broader 1 μm feature and longer wavelength position (~1.5 μm) for the turnover between the 1 and 2 μm features compared to the other Vestoids (~1.4 μm). These spectral differences imply a significant amount of olivine on the surface, driving the turnover to a longer wavelength. Spartacus' spectrum, while bearing a V-type classification, appears to be more olivine-rich than any measured HED specimen. This asteroid may contain material sampled from the mantle of Vesta. Alternatively, this object's "anomalous" spectrum compared with the spectra of other Vestoids may indicate that Spartacus has no relationship to Vesta. Primitive achondrites such as the lodranites and the acapulcoites (*e.g.*, McCoy *et al.*, 2000; Burbine *et al.*, 2001) are enriched in olivine relative to HED meteorites. However, these meteorites usually contain significant amounts of metallic iron (*e.g.*, McCoy *et al.*, 1997), which tends to suppress silicate absorption features, and, therefore, are probably not good compositional analogs for Spartacus since this asteroid has a relatively deep absorption band.

Determining Possible Causes of the Spectral Variations

The surprising results from these observations are that these Vestoids are much redder (higher peak reflectances) than Vesta and that some objects are redder than previously measured HED spectra (Gaffey, 1976). These differences are greater than any observational uncertainty in the continuum slope, which is on the order of $\pm$5%.

To understand these spectral differences, we have done a spectral study of a number of HED meteorites. Even though samples of these meteorites are available for detailed chemical and spectral analyses and reflectance spectra have been measured for a large number of these meteorites, there has been little work on correlating the diversity of HED spectra with specific mineralogical or compositional features. Here we explore the diversity of HED meteorite spectra and compare this diversity with that observed for the Vestoids. We implicitly assume that there are similarities in composition (making the HED meteorites the best analog planetary material to study in

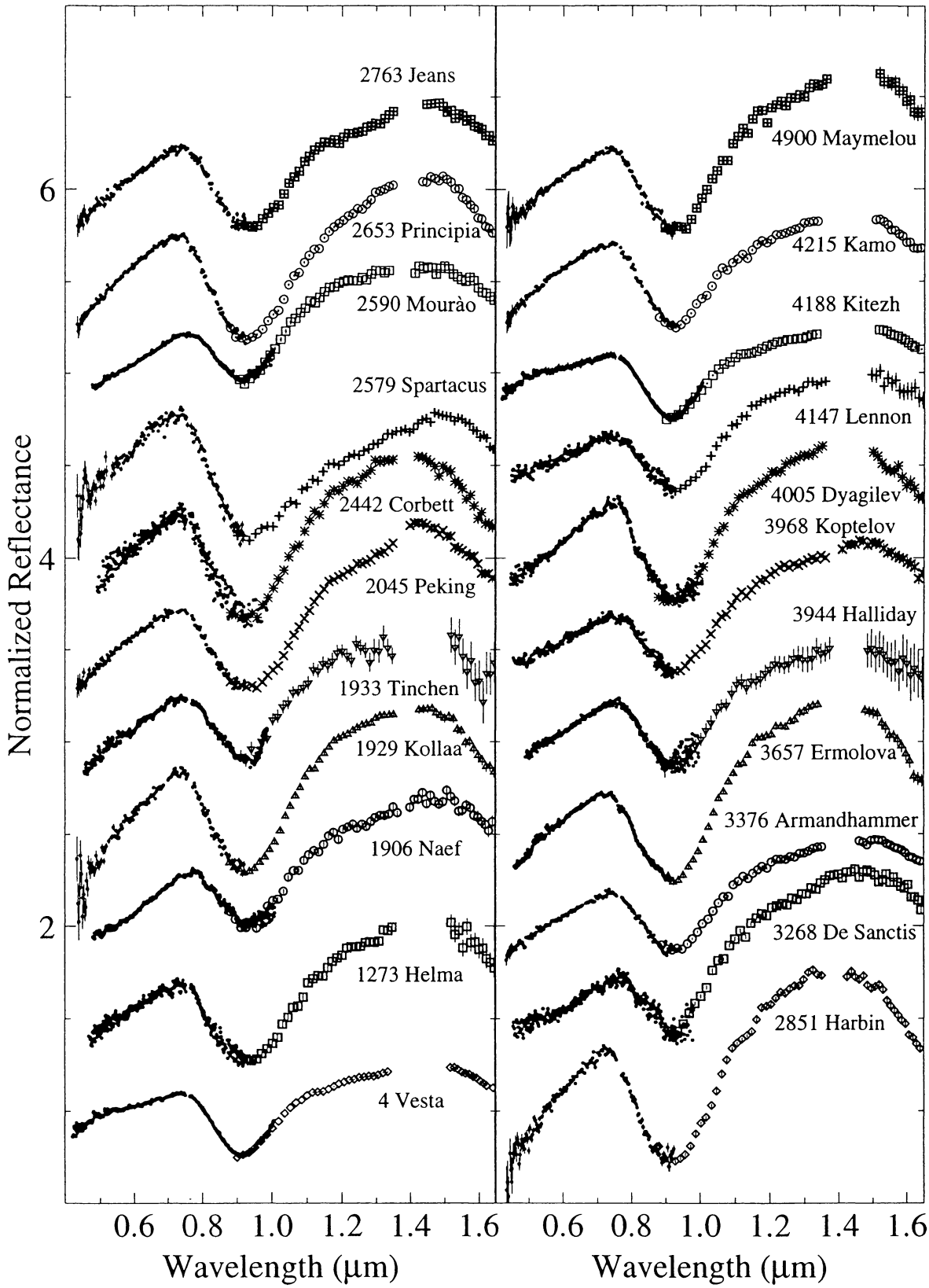

FIG. 2. Reflectance spectra from 0.4 to 1.65 μm of Vesta and the observed Vestoids. All spectra are normalized to unity at 0.55 μm and are offset by 0.5 in reflectance from each other for clarity. Objects are ordered by increasing asteroid number. Small dots are from SMASS I (Xu *et al.*, 1995) and SMASS II (Bus, 1999; Binzel and Bus, pers. comm.) and larger symbols are from SMASSIR. SMASS I data are plotted for 4 Vesta instead of SMASS II data since the SMASS I observations overlap better with the SMASSIR observations. Error bars are $\pm 1\sigma$.

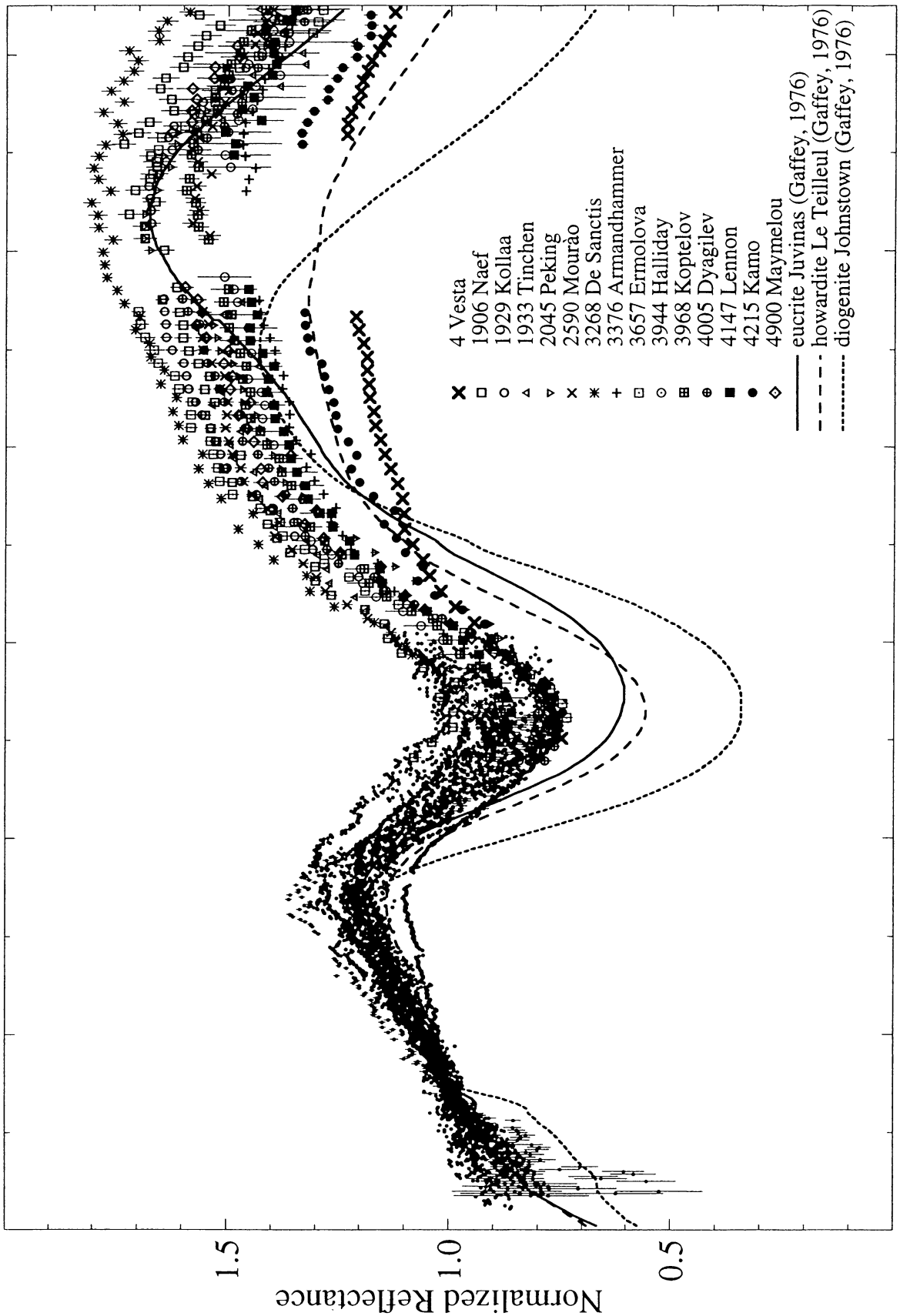

FIG. 3. Reflectance spectra from 0.4 to 1.65 μm of Vesta and the Vestoids in the HCM Vesta family *vs.* spectra of the eucrite Juvinas, howardite Le Teilleul, and diogenite Johnstown (Gaffey, 1976). All spectra are normalized to unity at 0.55 μm. Error bars are $\pm 1\sigma$.

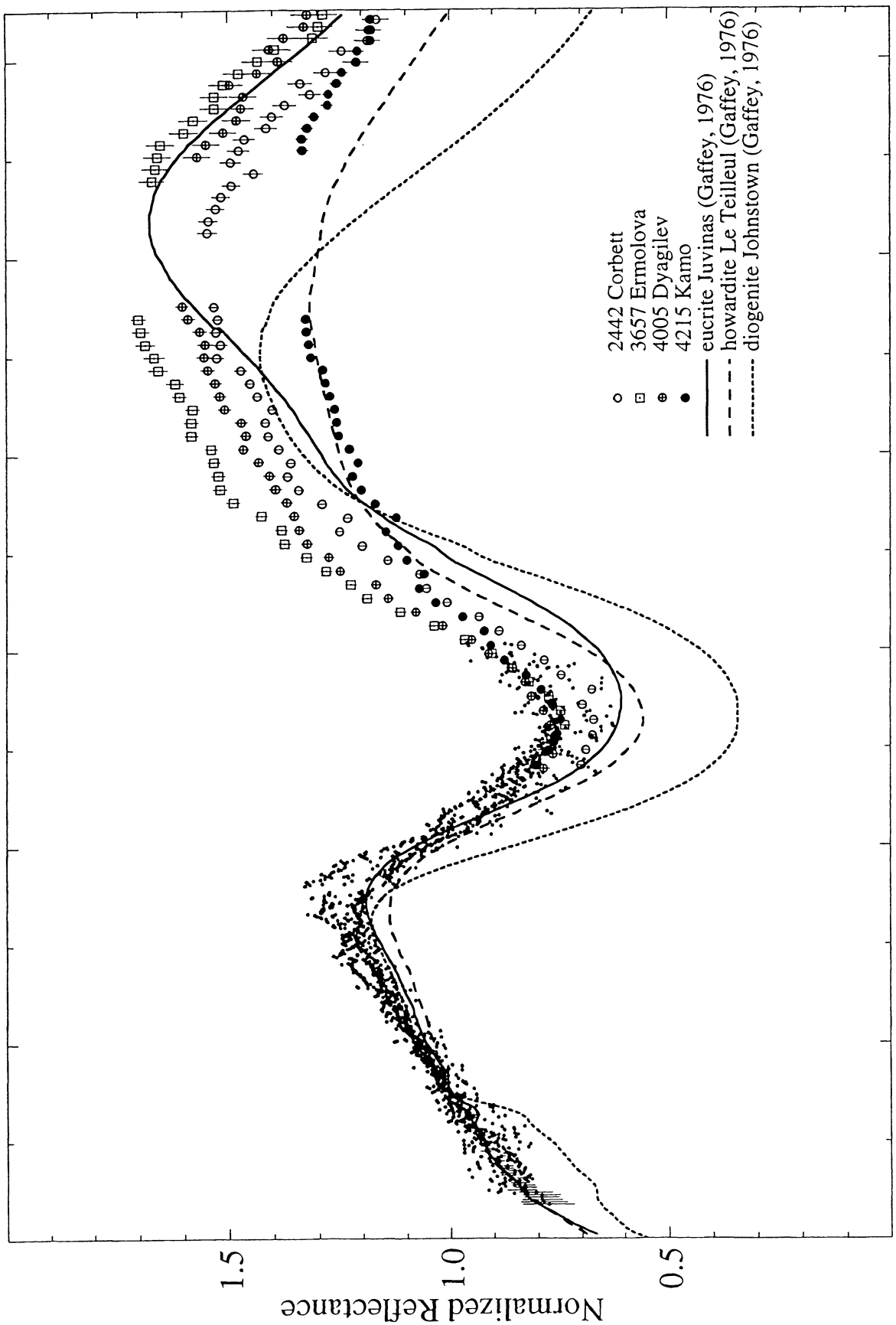

FIG. 4. Reflectance spectra from 0.4 to 1.65 μm of J asteroids *vs.* spectra of the eucrite Juvinas, howardite Le Teilleul, and diogenite Johnstown (Gaffey, 1976). All spectra are normalized to unity at 0.55 μm. Error bars are $\pm 1\sigma$.

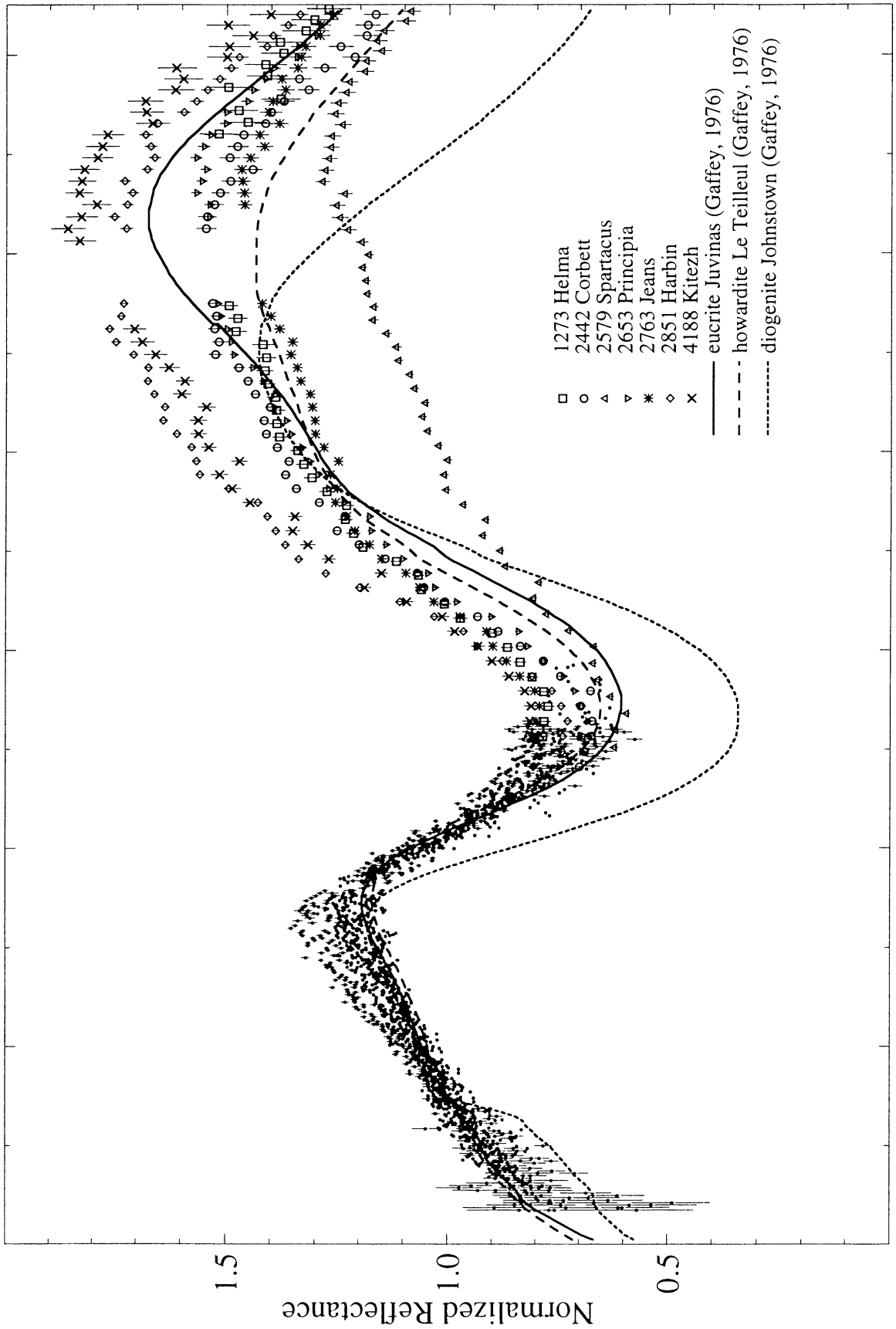

FIG. 5. Reflectance spectra from 0.4 to 1.65 μm of Vestoids outside the Vesta family *vs.* spectra of the eucrite Juvinas, howardite Le Teilleul, and diogenite Johnstown (Gaffey, 1976). All spectra are normalized to unity at 0.55 μm. Error bars are $\pm 1\sigma$.

the laboratory), but we do not require any assumption of an actual physical relationship.

ANALYTICAL TECHNIQUES

Room temperature reflectance spectra were obtained using the bidirectional spectrometer at the Keck/NASA reflectance experiment laboratory (RELAB) facility located at Brown University. The incident angle was 30° and the emission angle was 0°. The spectral coverage was 0.32 to 2.55 μm with a sampling interval of 0.01 μm and resolution of 0.001–0.006 μm for samples measured specifically for this work at RELAB. The exceptions are the very fine-grained (particle sizes less than 25 μm) samples of Bouvante (Hiroi, pers. comm.) and Padvarninkai (Hiroi *et al.*, 1995), which each had a sampling interval of 0.005 μm.

Low-temperature spectra for eucrite Elephant Moraine (EET) 83251 and howardite EET 87503 were acquired at the planetary geosciences/HIGP (Hawai'i Institute of Geophysics and Planetology) spectrometer facility at the University of Hawai'i at Manoa. The incident and emission angles were both 10.5°. The spectral coverage was ~0.36 to 2.5 μm with a sampling interval of 0.001 μm. The dispersion is 0.001 μm per element (10 Å per element). The temperature range was from ~120 to ~400 K.

Samples were either crushed to a powder with random particle sizes that should reflect the grain size of the material or crushed and dry sieved to determine an upper limit on the particle size. After the samples were pulverized, ~50 mg of material was removed for instrumental neutron activation analysis (INAA) measurements to determine bulk compositions except for the samples of Bouvante, EET 87503, and Macibini Clast 3. Previous INAA measurements were available for these three meteorites.

Bulk compositions of the meteorite samples were acquired at NASA JSC (Johnson Space Center) using standard INAA procedures. The ~50 mg samples plus standards and controls were encapsulated in pure silica glass tubes and irradiated at the research reactor facility of the University of Missouri at Columbia for 12 h at a flux of ~5.5×10^{13} neutrons/s/cm^2. Details of the JSC INAA lab analysis and data reduction procedures are described in Mittlefehldt and Lindstrom (1991) and Mittlefehldt *et al.* (1992). Only the calculated oxides (CaO, FeO, K_2O, and Na_2O) are listed in Table 4.

When average pyroxene compositions were not available in the literature, thin sections from the Smithsonian, NASA JSC, and the American Museum of Natural History (Bouvante) were probed. These thin sections were most likely not prepared from the same area where samples were extracted for spectral and INAA measurements, since the thin sections were almost all prepared right after the discovery of each meteorite years earlier.

Quantitative pyroxene analyses for EET 83251, EET 87542, EET 90020, Lewis Cliff (LEW) 87004, Pecora Escarpment (PCA) 82501, PCA 82502, and PCA 91007 were conducted using the JEOL JXA-8900R electron microprobe at the Smithsonian Institution. Analytical conditions were a 15 keV accelerating voltage, 20 nA beam current, and a fully-focused beam. Well-characterized minerals were used as standards and the data were corrected for absorption, fluorescence, and atomic number effects. Approximately 50 pyroxene analyses are averaged for each of the pyroxene compositions listed in Table 4.

Quantitative pyroxene analyses for Bouvante, Macibini clast 3, and EET 87503 were determined with the Cameca SX-100 electron microprobe at NASA JSC. Natural and synthetic materials were used as standards and the data were corrected for absorption, fluorescence, and atomic number effects. Average pyroxene compositions listed in Table 4 include ~140 analyses of Bouvante, ~40 analyses for Macibini clast 3, and ~300 analyses for EET 87503.

SPECTRAL VARIATIONS AMONG THE HOWARDITE, EUCRITE, AND DIOGENITE METEORITES

Previous Spectra

All HED meteorites have the distinctive 1 and 2 μm features due to pyroxene (Gaffey, 1976) (Fig. 6); however, there is a wide range in spectral properties among the HED meteorites. These HED spectra were measured for particle sizes between 30 and 300 μm at room temperature. Differences in the positions of absorption bands between the eucrites, howardites, and diogenites are due to variations in their pyroxene compositions. As noted earlier, eucrites have band minima that are shifted to longer wavelengths than the diogenites due to their more calcium- and iron-rich pyroxenes. There are also variations in the strength of the UV feature and the peak reflectance for each of the HED groups with the largest diversity among the eucrites. Eucrites have higher peak reflectances than the howardites and diogenites. These differences in peak reflectances are due to the more calcium-rich nature of the pyroxenes found in eucrites. These differences can be seen qualitatively in the higher peak reflectances of Ca-rich pyroxenes such as augite *vs.* Ca-poor pyroxenes such as hypersthene (*e.g.*, Clark *et al.*, 1993).

Plotted in bold lines in Fig. 6 are Sioux County and Juvinas, which are both brecciated eucrites with similar bulk compositions and mineral compositions (Kitts and Lodders, 1998). The two meteorites have almost identical mineral percentages (52 vol% pyroxene and 44% plagioclase) and average pyroxene compositions ($En_{37}Fs_{50}Wo_{12}$ for Sioux County and $En_{36}Fs_{49}Wo_{14}$ for Juvinas). These meteorites are also believed to have similar cooling and reheating histories (Takeda and Graham, 1991). However, Juvinas has a much stronger UV feature and a much higher peak reflectance than Sioux County. These spectral differences imply that a factor other than composition may be causing these large spectral variations among eucrites.

TABLE 4. Eucrites and the howardite that had spectra measured for this study.

Meteorite*	Notes†	Weathering‡	Pyroxene composition§			Bulk composition (wt%)#				Spectra measured	
			En (%)	Fs (%)	Wo (%)	CaO	FeO	K_2O	Na_2O	Particle sizes$	*T*
Monomict eucrites†											
ALH 85001	Mg-rich	A/B	66	32	2	7.6	14.3	<0.04	0.24	bulk	room
Bouvante	Stannern-trend	–	33	53	14	10.5	19.6	0.07	0.51	<25 μm, <250 μm, bulk	room
EET 87542	–	A	43	44	13	10.2	20.7	0.05	0.54	bulk	room
EET 90020	unbrecciated	A	33	53	13	10.0	20.7	0.03	0.40	bulk	room
PCA 82501	unbrecciated	A	36	54	9	10.4	18.6	0.06	0.58	bulk	room
PCA 82502	fine-grained	A	33	53	14	10.5	18.5	0.04	0.47	bulk	room
PCA 91007	–	A/Be	33	55	11	10.2	18.7	0.06	0.49	bulk	room
Polymict eucrites†											
ALH A76005	–	A	37	51	11	9.8	18.5	0.04	0.43	<250 μm, bulk	room
EET A79005	–	A	43	45	10	9.3	16.6	0.07	0.42	<250 μm, bulk	room
EET 83251	–	B	42	46	12	8.3	18.1	<0.06	0.48	<63 μm	~120–400 K
LEW 87004	–	A	44	45	11	8.9	18.8	0.03	0.42	bulk	room
Howardite†											
EET 87503	–	A	52	40	8	8.8	17.5	0.03	0.36	< 63 μm, 106–150 μm	~120–400 K
Impact melt breccia†											
Macibini clast 3	–	–	35	52	13	10.0	18.4	0.09	0.66	<63 μm	room

*The Bouvante spectrum (particle sizes less than 25 μm) was measured by Hiroi (pers. comm.) before this study commenced.
†Notes and meteorite types are from Buchanan (unpubl. data).
‡The weathering indicators for the Antarctic samples are from Grossman (1994). Weathering class of "A" indicate minor rustiness, "B" indicates moderate rustiness, "C" indicates severe rustiness, and "e" indicates evaporite minerals visible to the naked eye.
§Average pyroxene (En for enstatite, Fs for ferrosilite, and Wo for wollastonite) compositions for ALH A76005 are from Kitts and Lodders (1998), ALH 85001 are from Score and Mason (1986), EETA79005 are from Kitts and Lodders (1998), and Macibini clast 3 are from Buchanan *et al.* (2000) and Buchanan (unpubl. data). Average pyroxene compositions for Bouvante and EET 87503 are from electron microprobe analyses by done at NASA JSC for EET 83251, EET 87542, EET 90020, LEW 87004, PCA 82501, PCA 82502, and PCA 91007 are from analyses done at the Smithsonian. Average standard deviations for the analyses of the monomict eucrites are 2 mol% for the enstatite, 7 mol% for the ferrosilite, and 9 mol% for the wollastonite. Average standard deviations for the analyses of the polymict eucrites are 11 mol% for the enstatite, 8 mol% for the ferrosilite, and 7 mol% for the wollastonite. Standard deviations for the analyses of the howardite EET 87503 are 17 mol% for the enstatite, 14 mol% for the ferrosilite, and 8 mol% for the wollastonite and for the analyses of the impact melt breccia Macibini clast 3 are 2 mol% for the enstatite, 10 mol% for the ferrosilite, and 11 mol% for the wollastonite.
#Weight percents of CaO (error bars of approximately ±0.5), FeO (error bars of approximately ±0.2), K_2O (error bars of approximately ±0.01), and Na_2O (error bars less than ±0.01) were calculated from INAA measurements of powdered samples. INAA data for Bouvante are from Kitts and Lodders (1998), EET 87503 are from Mittlefehldt and Lindstrom (pers. comm.), and Macibini clast 3 are from Buchanan *et al.* (2000).
$Bulk samples were just crushed to a powder with random particle sizes that should reflect the grain size of the material.

New Spectra

The eucrites and howardites for which reflectance spectra were measured for this study are listed in Table 4. The spectral characteristics of the bulk eucrite samples (where the material was only crushed to a powder and not sieved) are shown in Fig. 7. These eucrite spectra are similar to those measured by Gaffey (1976) with distinctive 1 and 2 μm features due to pyroxene and a wide variation in the strength of the UV feature and in the peak reflectance. There is a much larger variation in spectral slopes for the measured monomict eucrites than the polymict ones. The ~0.5065 μm feature discussed by Vilas *et al.* (2000) are present in the spectra. In these eucrites, the strength of this feature varies from ~2% to practically negligible. Further work needs to be done to quantify what is controlling the strength of this feature in the spectra of HED meteorites.

Two meteorites (Allan Hills (ALH) 85001 and EET 90020) have spectra that appear "unusual" and are specifically labeled in Fig. 7. The Mg-rich monomict eucrite ALH 85001 is spectrally blue (reflectance tends to decrease with increasing

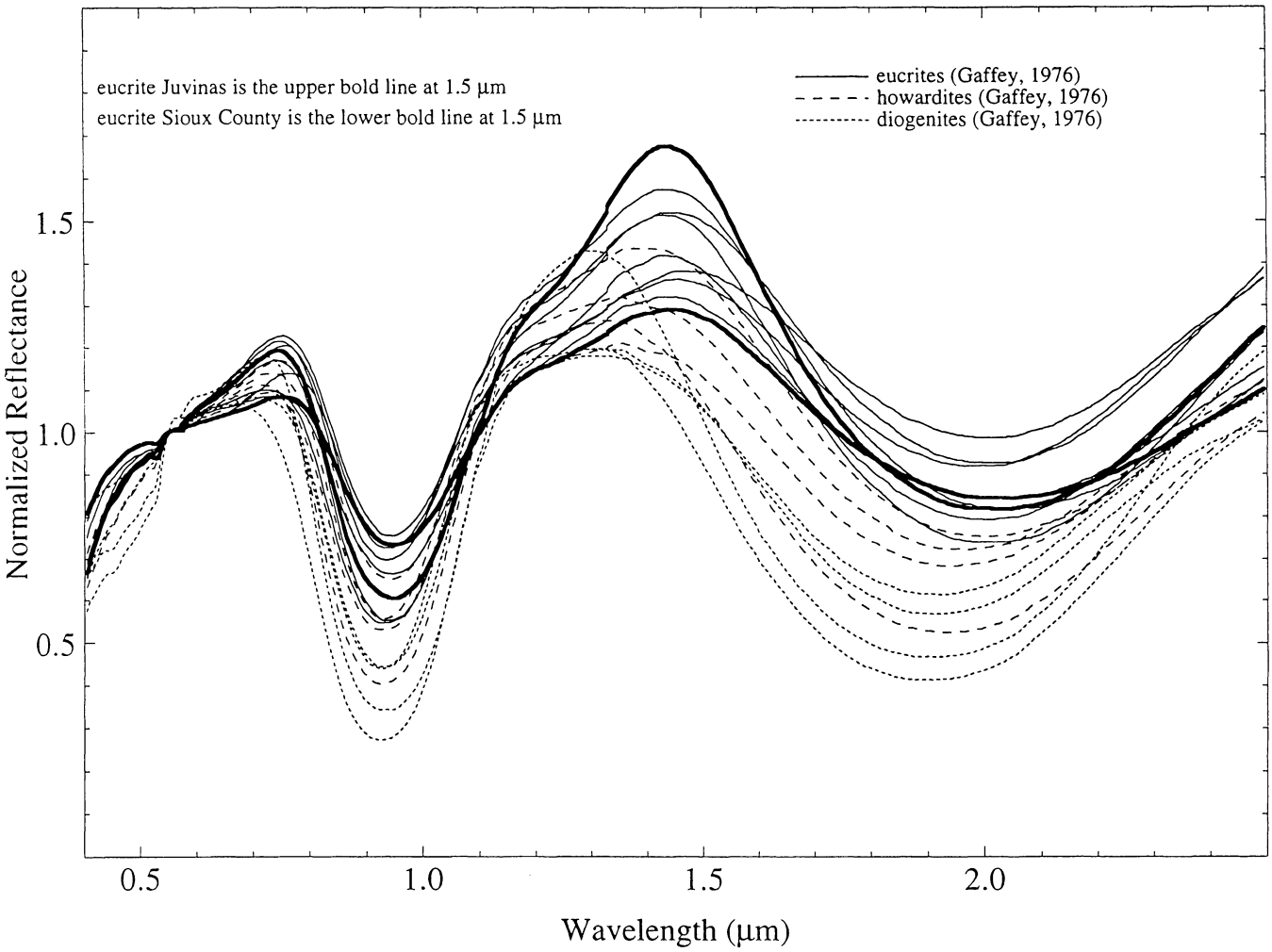

FIG. 6. Reflectance spectra from 0.4 to 2.5 μm of eucrites, howardites, and diogenites from Gaffey (1976). Two eucrites (Juvinas and Sioux County) with very similar compositions are plotted in bold lines.

wavelength). It is unclear if this "blueness" is due to this meteorite's Mg-rich pyroxene composition and/or the presence of relatively large grains (~3 mm), which are found in the fine-grained groundmass of this meteorite (Score and Mason, 1986). The very strong UV feature of EET 90020 is indicative of terrestrial alteration. Visual examination of the measured powder showed it to have an orange tinge, which is consistent with the effects of terrestrial weathering.

We compiled a range of spectral parameters (Table 5) for spectra not published previously to try to determine the cause of spectral variations. These parameters include Band I minima, Band I centers, Band II minima, the position of the ~1.4 μm peak, the ~1.4 μm peak reflectance, and the reflectance at 0.55 μm (visual albedo). The Band I minima and centers are virtually indistinguishable within $\pm$0.01 μm error bars for the measured eucrites and the howardite. The visual albedo can be seen to increase as the particle size decreases. More spectral variation can be seen in the positions of the Band II minima (and to a lesser extent, the positions of the ~1.4 μm peaks). The monomict eucrites, excluding ALH 85001, tend to have Band II minima at longer wavelengths than the polymict eucrites owing to their slightly more Ca- and Fe-rich average pyroxene compositions.

One unexpected spectral variation is that the Band II minimum tends to move to shorter wavelengths (Table 5) as a sample is sieved to smaller particle sizes. This band minimum wavelength shift along with grain size is likely caused by a change in the continuum. Finer samples have a redder continuum, which makes its band minimum appear shorter in wavelength.

Particle Size

There are significant differences in spectral characteristics between bulk-powder eucrite samples and those sieved to smaller particle sizes (Fig. 8). As particle size decreases, the

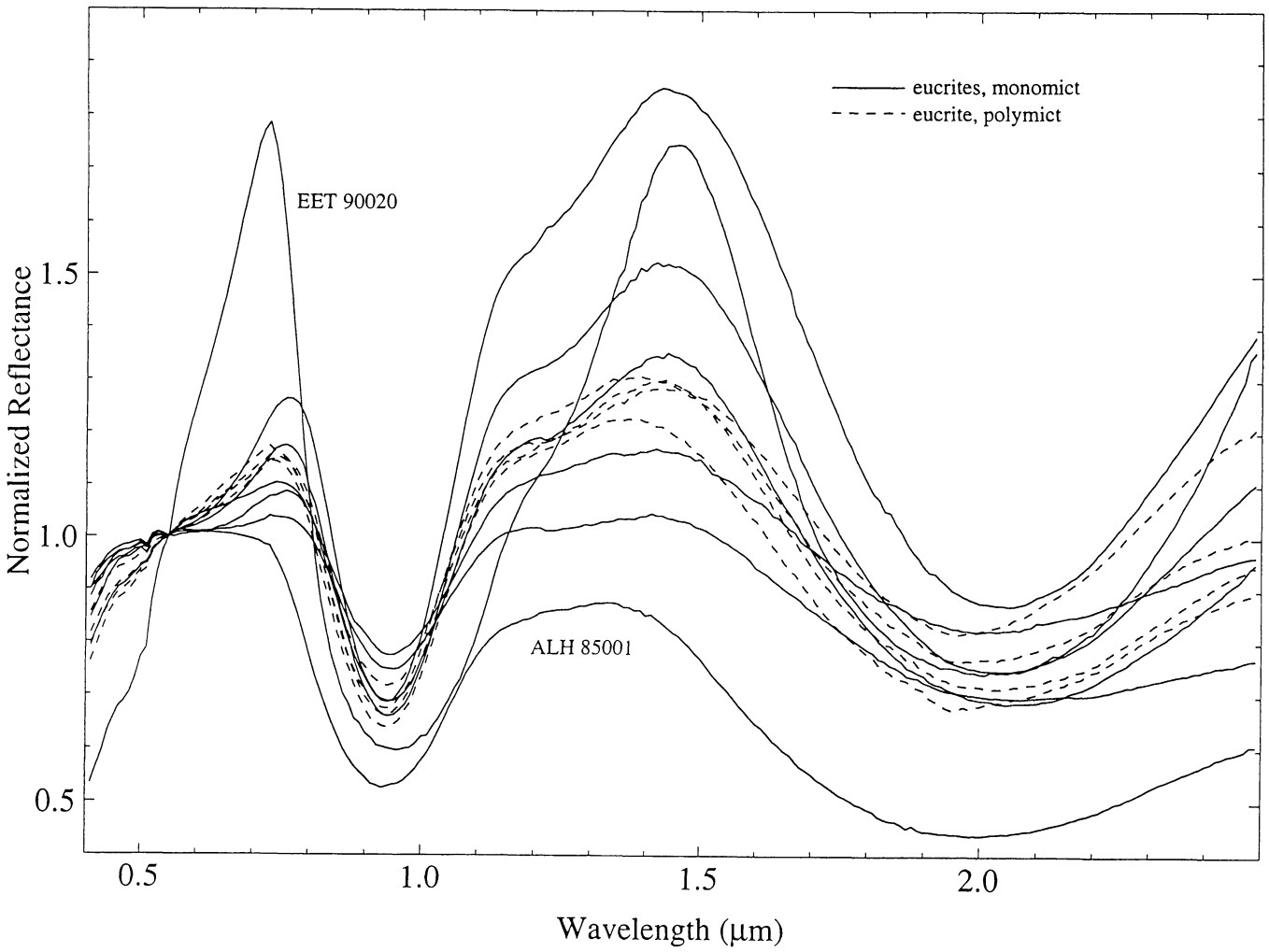

FIG. 7. Reflectance spectra from 0.4 to 2.5 μm of bulk-powder eucrite samples. A wide variety of spectral slopes can be seen for these samples. All spectra are normalized to unity at 0.55 μm.

UV features tend to become stronger and the spectra tend to become redder as seen by their higher peak reflectances. These increases in reddening are most likely due to the reduction in size of the average particle. Larger particles have larger internal path lengths so photons are more likely to be absorbed into the material than to be scattered (Clark, 1999). Decreasing the particle size will increase the probability, which tends to increase with increasing wavelength for these samples, that light will be reflected back to the observer. Other meteorite types that tend to significantly redden as samples are sieved to smaller particle sizes include the carbonaceous chondrites (Johnson and Fanale, 1973).

These spectral differences for eucrites are not likely due to the preferential enrichment of pyroxene or plagioclase during the sieving process. Pyroxene dominates the spectral properties of pyroxene-plagioclase mixtures (Adams, 1974; Crown and Pieters, 1987) unless the assemblage is almost entirely plagioclase. Plagioclase is mechanically weaker than pyroxene so plagioclase would be more likely to be enriched in the finer-grained samples (*e.g.*, Hiroi *et al.*, 1995). Also, the spectral slope of pyroxene-plagioclase mixtures (Crown and Pieters, 1987) decreases with increasing plagioclase content.

The Bouvante spectrum for the particle size less than 25 μm has the reddest slope of any measured HED with a normalized reflectance peaking at a value of almost 2.0, which is redder than any measured Vestoid. The width of the 1 μm feature also becomes much narrower for this particle size (less than 25 μm). The feature centered at ~0.65 μm could be due to ilmenite ($FeTiO_3$) (Clark *et al.*, 1993), which was observed as relatively coarse-grained (a few hundred microns) inclusions in Bouvante. Pyroxenes, especially augites, also show a band around ~0.64 μm that appear to be due to minor elements (such as chromium) (*e.g.*, Hiroi *et al.*, 1985) in its crystal structure.

The reason why this Bouvante sample has the reddest reflectance spectrum of any measured eucrite may be due to the high calcium content of its pyroxenes compared to the other

TABLE 5. Spectral parameters for the eucrites and the howardite measured in this study.

Meteorite*	Particle sizes	T	Pyroxene composition†			Band I minimum‡ (μm)	Band I center‡§ (μm)	Band II minimum‡ (μm)	~1.4 μm peak‡ (μm)	~1.4 μm peak reflectance#	Reflectance at 0.55 μm$
			En (%)	Fs (%)	Wo (%)						
Monomict eucrites											
ALH 85001	bulk	room	66	32	2	0.93	0.93	2.00	1.34	0.88	0.26
Bouvante	<25 μm	room	33	53	14	0.94	0.95	2.02	1.46	1.98	0.27
Bouvante	<250 μm	room	33	53	14	0.95	0.95	2.03	1.44	1.61	0.20
Bouvante	bulk	room	33	53	14	0.94	0.95	2.05	1.44	1.35	0.19
EET 87542	bulk	room	43	44	13	0.94	0.95	2.00	1.42	1.17	0.28
PCA 82501	bulk	room	36	54	9	0.95	0.95	2.02	1.41	1.05	0.23
PCA 82502	bulk	room	33	53	14	0.94	0.95	2.05	1.43	1.85	0.17
PCA 91007	bulk	room	33	55	11	0.94	0.93	2.02	1.42	1.53	0.17
Polymict eucrites											
ALHA76005	<250 μm	room	37	51	11	0.94	0.94	1.99	1.41	1.54	0.23
ALHA76005	bulk	room	37	51	11	0.94	0.94	2.02	1.41	1.30	0.19
EETA79005	<250 μm	room	43	45	10	0.93	0.94	1.95	1.39	1.42	0.26
EETA79005	bulk	room	43	45	10	0.94	0.94	1.98	1.39	1.23	0.20
EET 83251	<63 μm	200 K	42	46	12	0.93	0.93	1.97	1.39	1.44	0.27
EET 83251	<63 μm	300 K	42	46	12	0.94	0.94	1.97	1.38	1.43	0.27
LEW 87004	bulk	room	44	45	11	0.94	0.94	1.96	1.43	1.28	0.23
Howardite											
EET 87503	<63 μm	200 K	52	40	8	0.93	0.92	1.94	1.38	1.29	0.27
EET 87503	<63 μm	300 K	52	40	8	0.93	0.93	1.96	1.38	1.34	0.25
EET 87503	106–150 μm	200 K	52	40	8	0.94	0.93	1.96	1.37	1.06	0.19
EET 87503	106–150 μm	300 K	52	40	8	0.93	0.93	1.99	1.37	1.08	0.18
Impact melt breccia											
Macibini clast 3	<63 μm	room	35	52	13	0.94	0.95	1.98	1.45	1.40	0.21

*EET 90020 is not included in the table since weathering has noticeably affected its spectrum.
†Average pyroxene compositions are from Table 4.
‡Error bars for the band positions are about ±0.01 μm, which is the sampling interval for most of the RELAB spectra.
§The band centers are the minima after a linear continuum has been divided out of each spectrum.
#The reflectance at the ~1.4 μm peak is calculated from spectra that have been normalized to unity at 0.55 μm. The error bars for the reflectances are less than ±0.01.
$The reflectance at 0.55 μm is equivalent to the visual albedo. The error bars for the reflectances are less than ±0.01.

eucrites coupled with its very fine-particle size. As mentioned earlier, Ca-rich pyroxenes tend to have higher peak reflectances than Ca-poor pyroxenes. The two samples with the reddest spectra (monomict eucrites Bouvante and PCA 82502) (Table 5) have the highest average wollastonite contents (Wo_{14}) of the measured samples. Even though PCA 82502 was measured as a bulk sample, it is very fine grained (Schwarz and Mason, 1983) and should have broken into relatively small fragments during the crushing process.

Glass

A few howardites have been found to have glass contents as high as ~15–20 vol% (*e.g.*, Desnoyers and Jerome, 1977; Olsen *et al.*, 1987, 1990). However, generally glass represents a very small proportion (<<1%) of the volume of known HED meteorites. Experiments by Wasson *et al.* (1997) suggested that the formation of glass in HED meteorites, through laser impulse irradiation, can redden (by ~30%) HED spectra. Irradiation by a laser is used to duplicate the energy supplied by the impact of micrometeorites on the surface of an asteroid. Yamada *et al.* (1999) obtained reddening and band reduction without forming glass for their laser experiments on terrestrial pyroxenes.

To determine the effects of glass found naturally in HED meteorites, a spectrum (Fig. 9) was measured for an impact melt clast in the eucritic breccia Macibini (Buchanan *et al.*, 2000) and compared to spectra of previously measured samples of the eucrite Padvarninkai (Gaffey, 1976; Hiroi *et al.*, 1995). The Macibini clast is approximately 50% devitrified glass and 50% silicates. Padvarninkai is one of the most heavily shocked eucrites known (Yamaguchi *et al.*, 1993) with most plagioclase

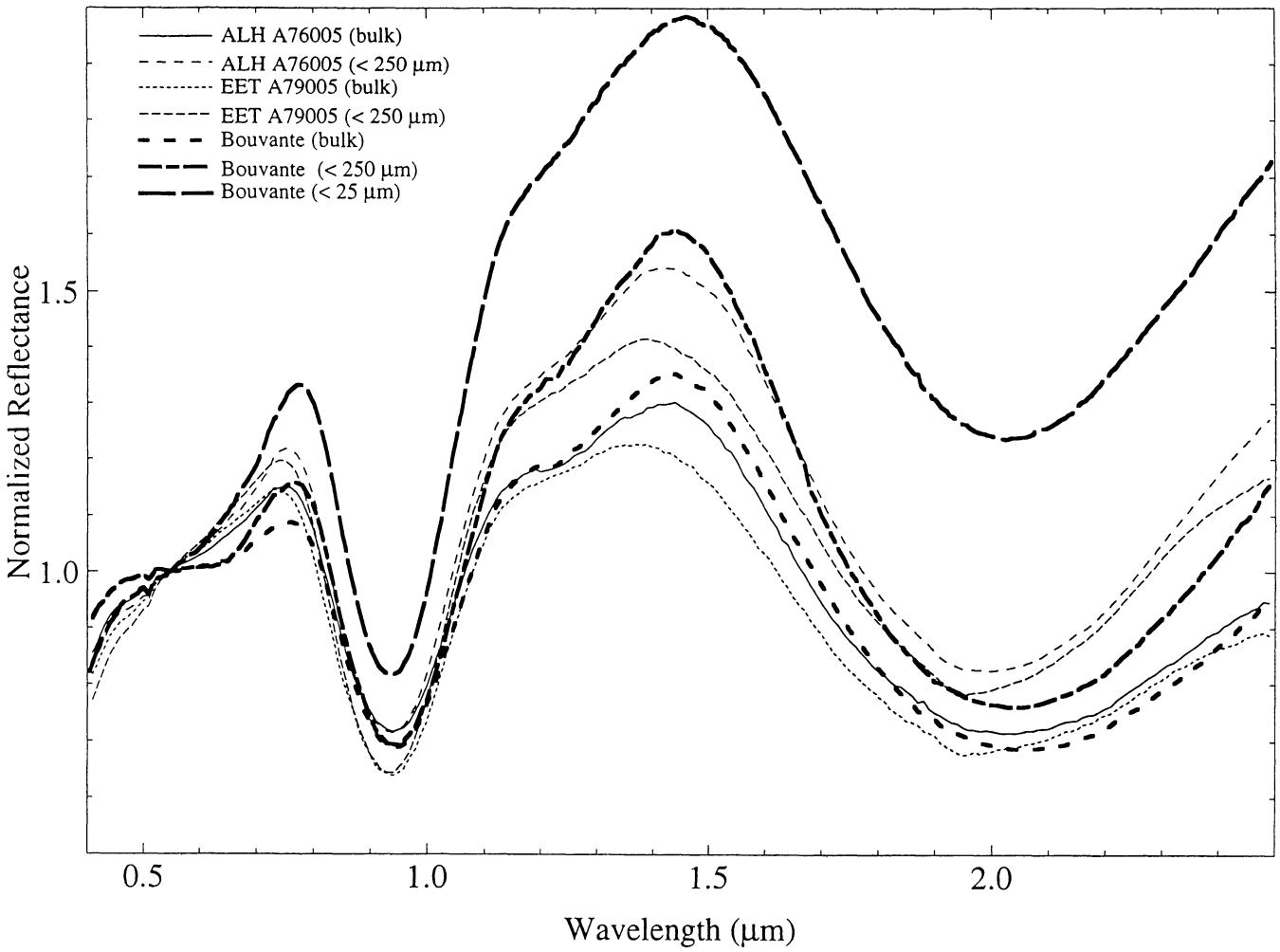

FIG. 8. Reflectance spectra from 0.4 to 2.5 μm of different particle sizes (bulk powder and less than 250 μm) of eucrites ALHA76005, and EETA79005 and different particle sizes of Bouvante (bulk powder, less than 250 μm, and less than 25 μm). Bouvante is plotted in bold lines for clarity. Spectral slope increases with decreasing grain size. All spectra are normalized to unity at 0.55 μm.

converted to maskelynite and containing a significant amount of impact melt glass. The finer-grained Padvarninkai (Hiroi *et al.*, 1995) has a much narrower 1 μm feature and a much weaker band depth, due to its smaller particle size. None of these glass-rich meteorites appear significantly reddened.

Temperature

The surface temperature of asteroids at Vesta's location in the belt is ~200 K (Hinrichs *et al.*, 1999), assuming a fine-grained regolith. Low (200 ± 5 K) and room (300 ± 2 K) temperature spectra of a eucrite and a howardite are shown in Fig. 10. The considerable amount of scatter at ~0.9 and ~2.4 μm is due to low counting statistics.

The spectral variations between the eucrite spectra at these two temperatures are very slight. The largest variation is in the 1 μm band width, which shrinks by ~10% with decreasing temperature. The spectral variations with decreasing temperature in the howardite spectra are primarily a decrease in strength of the UV feature and a decrease in value of the peak reflectance. However, the spectral differences for the howardite due to grain size are much larger than any differences due to temperature (Fig. 10).

Nanophase Reduced Iron

One process known to redden lunar soils (*e.g.*, Pieters *et al.*, 1993; Noble *et al.*, 2001; Taylor *et al.*, 2001) is the production of nanophase reduced iron from a combination of vapor deposition from micrometeorite impacts and irradiation effects. However, this process also reduces significantly the strength of the absorption bands, which is not consistent with the relatively strong 1 μm features of the Vestoids. Yet, a low degree of "space weathering" can still exist on Vestoids, which

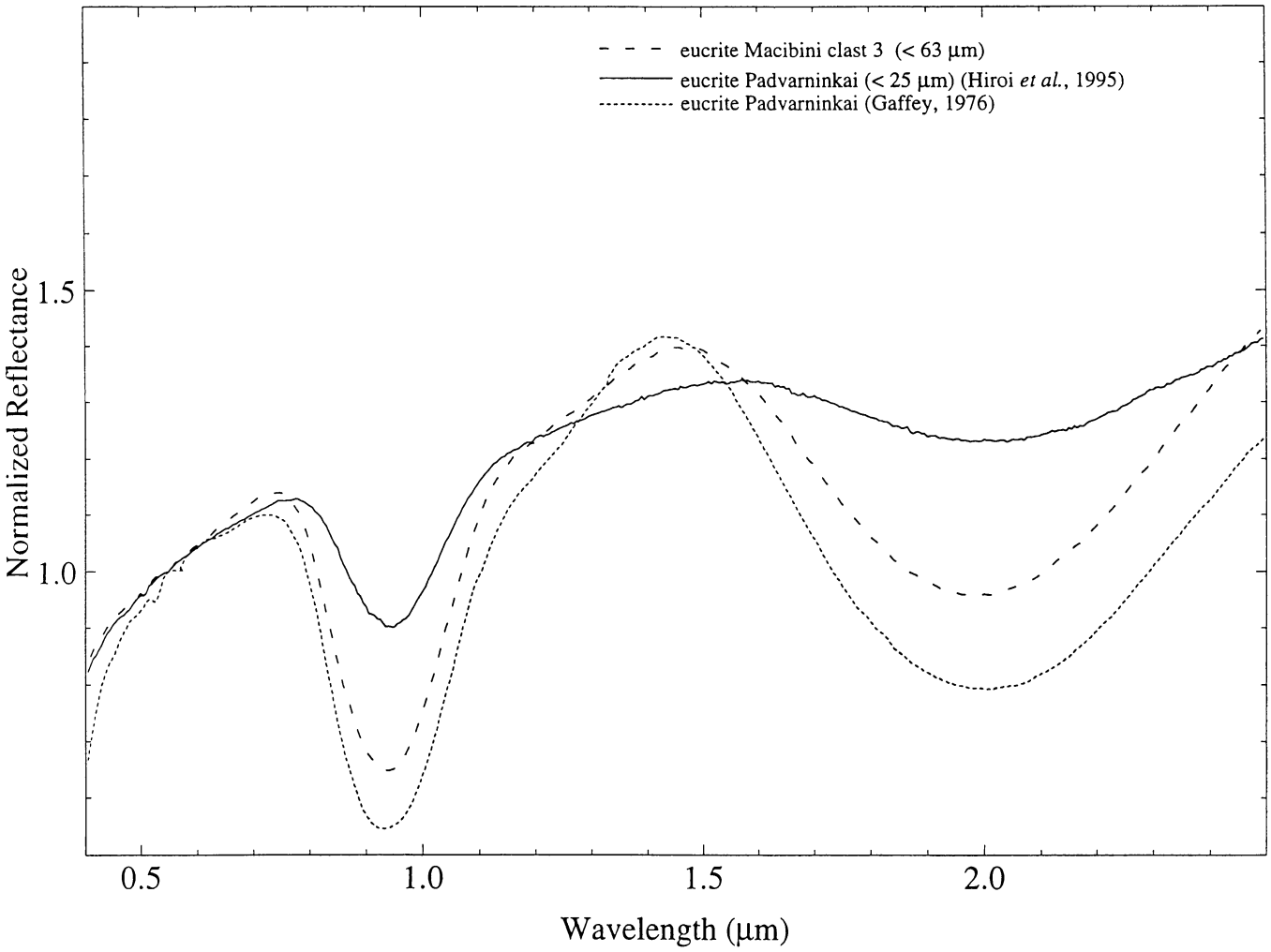

FIG. 9. Reflectance spectra from 0.4 to 2.5 μm of eucrite Macibini clast 3 (particle sizes less than 63 μm) and the eucrite Padvarninkai. The Padvarninkai spectrum for particle sizes less than 25 μm is from Hiroi *et al.* (1995) and the coarser (particle sizes between approximately 30 and 300 μm) Padvarninkai spectrum is from Gaffey (1976). All spectra are normalized to unity at 0.55 μm.

could erase the ~0.5065 band of some Vestoids (Vilas *et al.*, 2000). Compared to a body with an ordinary chondrite composition, Pieters *et al.* (2000) argue that the production of nanophase reduced iron would be much slower on a body with an HED-like composition due to a lack of abundant metallic iron in the regolith.

ARE THESE VESTOIDS FRAGMENTS OF VESTA?

All observed Vesta family members have spectra that fall intermediate between the spectra of eucrites with very-fine particle sizes and eucrites and howardites with coarser particle sizes. All of these objects have the distinctive 1 μm feature due to pyroxene plus the start of the 2 μm feature. The reddest Vestoids have spectra consistent with eucritic material that has average particle sizes that are on the order of 25 μm or finer. Eucrites with the reddest spectra tend to have pyroxenes with the highest average wollastonite contents. Other factors such as surface temperature and glass content will affect the spectra of HED material, but only decreasing the particle size appears to redden eucrite spectra to the extremes found in some of the Vestoids.

One nagging question is "why are the Vestoids redder than Vesta?" Vesta's surface would be expected to be much older than those of the Vestoids and, therefore, much finer grained since it would have experienced a much larger degree of micrometeorite impacts. However, the redder spectra of the Vestoids would argue that they have finer-grained surfaces. One possibility is that Vesta's much higher gravity can retain bigger particles on its surface than the Vestoids. Another possibility is that the Vestoids represent the original finer-grained surface of Vesta that was more extensively gardened early in solar system history (or were, perhaps, finer grained because they represent quickly cooled surficial flows), whereas the present surface of Vesta is more recent and may represent coarser-grained igneous rocks. In this scenario, impact processes have stripped off the original surface of Vesta. A third possibility is

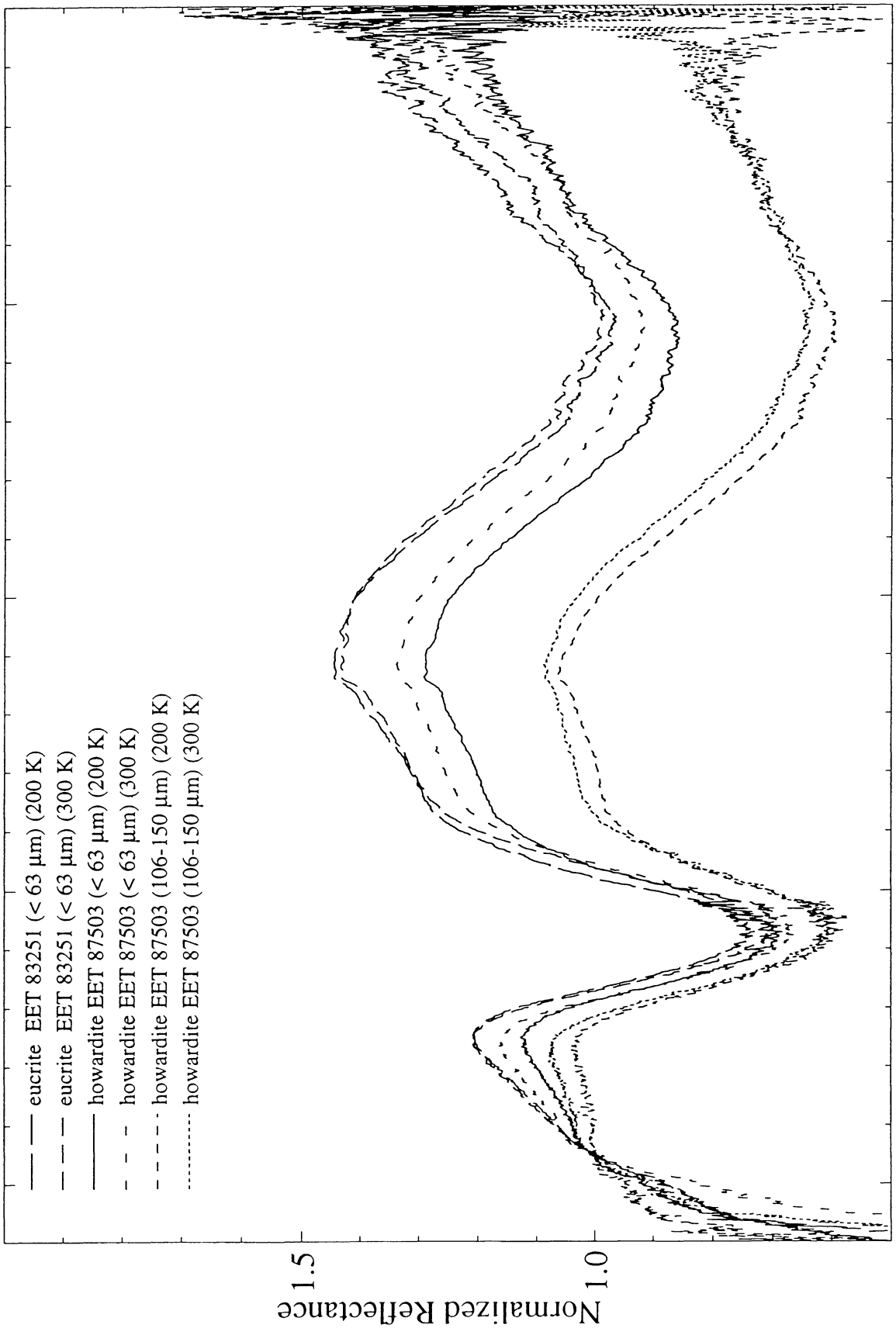

FIG. 10. Reflectance spectra from 0.4 to 2.5 μm of eucrite EET 83251 (particle sizes less than 63 μm) and howardite EET 87503 (particle sizes less than 63 μm and between 106 and 150 μm) at low (200 ± 5 K) and room (300 ± 2 K) temperatures. All spectra are normalized to unity at 0.55 μm.

that Vesta is fine grained (Hiroi *et al.*, 1994) and is not spectrally red due to a large proportion of Ca-poor pyroxenes from diogenitic material on the surface.

Observed non-family members also have spectra that fall intermediate between the spectra of eucrites with very-fine particle sizes and eucrites and howardites with coarser particle sizes except for one object (2579 Spartacus). This implies that the "actual" Vesta family extends beyond the statistically defined Vesta family. This is not a surprise since the distances in proper element space used to define each dynamical family are somewhat arbitrary. The broader 1 μm feature of Spartacus' spectrum seems to indicate that it is more olivine-rich than a typical Vestoid. It is impossible to know if Spartacus is a fragment of Vesta that contains mantle material or is altogether unrelated to Vesta.

The apparent absence of Vestoids resembling diogenites may be due to the difficulty in ejecting fragments of observable sizes (*e.g.*, 10 km in diameter) that contain substantial amounts of diogenitic material on their surfaces. Smaller fragments of diogenitic material must be easier to eject since of the ~400 known HED meteorites (Grady, 2000), ~25% have been classified as diogenites and ~25% as howardites. By mass, only ~15% of HED material have been classified as diogenites and ~15% as howardites.

Miyamoto and Takeda (1994) estimated that the HED parent body had a eucritic crust that extended to a depth of ~8 km by numerically solving the diffusion equation of Ca atoms required for augite lamella growth in pyroxenes from the cumulate eucrite Moore County. Estimates for the formation region of the diogenites on Vesta vary from depths of ~23 km (Ruzicka *et al.*, 1997) to ~130 km (Grove and Bartels, 1992), depending on the fractional crystallization model and pressures needed to produce the diogenites from assumed initial compositions. Impacts on Vesta, such as the one that produced the 460 km diameter crater (Thomas *et al.*, 1997b), are expected to sample depths of ~30–40 km (Asphaug, pers. comm.). This may not be deep enough to excavate ~10 km fragments with surfaces entirely composed of diogenitic material.

Since Vesta has a spectrum similar to howardites (*e.g.*, Hiroi *et al.*, 1994; Gaffey, 1997) and almost all of the observed Vestoids have spectra similar to eucrites or howardites, the simplest scenario for the formation of the Vestoids appears to be one where these small objects are fragments of Vesta. Theoretical calculations (*e.g.*, Marzari *et al.*, 1996; Asphaug, 1997) have no difficulty in modeling the creation of the Vesta family by the ejection of fragments from Vesta. The formation of the 460 km diameter impact crater on Vesta (Thomas *et al.*, 1997b) would have ejected ~10^6 km^3 of material, which is dramatically more than the volume of the over 200 small asteroids that comprise the Vesta family.

Other possibilities for forming the Vestoids appear unlikely. We cannot rule out a scenario (Wasson *et al.*, 1996) where fragments of a projectile that had a grazing impact with Vesta are coated with "Vesta dust" and, thus, appear "Vesta-like". However, the identification of the 460 km crater on Vesta argues very persuasively that a very substantial volume of material from Vesta has been excavated and ejected. The possibility that the Vestoids are fragments of a destroyed basaltic parent body located near Vesta appears improbable. The disruption of another basaltic body near Vesta would be expected to release many more mantle fragments than basaltic ones (*e.g.*, Burbine *et al.*, 1996). This is not the case for the Vesta family, which is dominated by asteroids that appear pyroxene-rich.

However, we note that over the age of the solar system, Vesta is probably not the only object that had a "basaltic" surface since compositional groupings of iron meteorites imply the disruption of at least ~70 differentiated parent bodies (Wasson, 1995). Crustal fragments of other differentiated bodies are generally thought to have been pulverized to sizes below our observational limits for spectroscopy (*e.g.*, Burbine *et al.*, 1996). An object (1459 Magnya) with a "Vesta-like" spectrum (Lazzaro *et al.*, 2000) has been identified at 3.15 AU, which is too far to be easily related to Vesta at 2.36 AU. Magnya is estimated to have a diameter between ~15 and ~30 km, depending on its visual albedo. Magnya appears to be evidence that fragments of other differentiated objects with "basaltic" surfaces are indeed still present in the asteroid belt at spectrally observable sizes and could possibly be supplying meteorites to Earth.

By the arguments put forth by Consolmagno and Drake (1977), Vesta appears to be the most likely source of the HED meteorites due to its apparent presence in the asteroid belt as the only large body surviving with its original, intact "basaltic" crust. Recent dynamical studies (*e.g.*, Bottke *et al.*, 2000; Vokrouhlický and Farinella, 2000) argue that all asteroids in the inner main belt are potential meteorite parent bodies. However, both Bottke *et al.* (2000) and Vokrouhlický and Farinella (2000) find that their theoretical models for producing ejecta from Vesta and delivering these fragments to Earth appear relatively consistent with the distribution of cosmic-ray exposure ages among the HED meteorites (Welten *et al.*, 1997). Cosmic-ray exposure ages measure the time interval in space that a meteoroid has spent exposed within a meter of the surface on its parent body or as a meter-sized object by determining the abundance of a cosmogenically-produced nuclide (*e.g.*, ^{21}Ne). But to conclusively determine if Vesta is the parent body of the majority of the HED meteorites, a sample return mission from Vesta is probably needed.

Acknowledgments–Results from this paper were part of the Ph.D. thesis of T. H. B. at the Massachusetts Institute of Technology. This research was primarily supported by NASA grant NAG5-3939 and NSF grant AST-9530282 to R. P. B. Other researchers were supported by a variety of grants including NASA RTOP (Research and Technology Operating Plan) #344-31-10-17 (David Lindstrom, P. I.), National Research Council-JSC Research Associateship (P. C. B.), Smithsonian Postdoctoral Fellowship (T. H. B.), NASA grant NAG5-4490 (T. J. M., P. I.), NAG5-4212 (Klaus Keil, P. I.), NAG5-7609-001 (Trevor Ireland, P. I.), and Danish Natural Science Research Council (A. M.). RELAB is a multi-user facility supported by NASA grant NAG5-3871.

The authors thank H. Y. McSween, Jr. and Faith Vilas for helpful reviews that greatly improved the manuscript, Carlé Pieters for her work as associate editor, and D. W. Mittlefehldt for his expertise in INAA analyses and some unpublished data. The authors would also like to thank the Meteorite Working Group and American Museum of Natural History for providing samples, and the Center for Earth and Planetary Studies at the National Air and Space Museum of the Smithsonian Institution for providing computer support. The proper elements were taken from a database compiled by the Space Mechanics Group at the University of Pisa. The family memberships were taken from a database compiled by the Planetological Group of the Torino Astronomical Observatory. T. H. B., R. P. B., and S. J. B. were all visiting astronomers at the Infrared Telescope Facility, which is operated by the University of Hawai'i under contract to the National Aeronautics and Space Administration. This is HIGP publication number 1135 and SOEST publication number 5345. This paper is dedicated to the memory of Pye Burbine (1982–2001).

Editorial handling: C. M. Pieters

REFERENCES

ADAMS J. B. (1974) Visible and near-infrared diffuse reflectance spectra of pyroxenes as applied to remote sensing of solid objects in the solar system. *J. Geophys. Res.* **87**, 4829–4836.

ASPHAUG E. (1997) Impact origin of the Vesta family. *Meteorit. Planet. Sci.* **32**, 965–980.

BELL J. F. (1998) The Vesta asteroid family: Fact or fiction? (abstract). *Lunar Planet. Sci.* **29**, #1851, Lunar and Planetary Institute, Houston, Texas, USA (CD-ROM).

BINZEL R. P. (2001) Forging the fourth link between planetary worlds: Vesta and the HEDs. *Meteorit. Planet. Sci.* **36**, 479–480.

BINZEL R. P. AND XU S. (1993) Chips off of asteroid 4 Vesta: Evidence for the parent body of basaltic achondrite meteorites. *Science* **260**, 186–191.

BOTTKE W. F., JR., RUBINCAM D. P. AND BURNS J. A. (2000) Dynamical evolution of main belt meteoroids: Numerical simulations incorporating planetary perturbations and Yarkovsky thermal forces. *Icarus* **145**, 301–331.

BOWELL E., HAPKE B., DOMINGUE D., LUMME K., PELTONIEMI J. AND HARRIS A. W. (1989) Application of photometric models to asteroids. In *Asteroids II* (eds. R. P. Binzel, T. Gehrels and M. S. Matthews), pp. 524–556. Univ. Arizona Press, Tucson, Arizona, USA.

BUCHANAN P. C., LINDSTROM D. J., MITTLEFEHLDT D. W., KOEBERL C. AND REIMOLD W. U. (2000) The South African polymict eucrite Macibini. *Meteorit. Planet. Sci.* **35**, 1321–1331.

BURBINE T. H., JR. (2000) Forging asteroid-meteorite relationships through reflectance spectroscopy. Ph.D. thesis, Massachusetts Institute of Technology, Cambridge, Massachusetts, USA. 303 pp.

BURBINE T. H. AND BINZEL R. P. (1997) SMASSIR measurements of Vesta chips: Evidence for weathering? (abstract). *Bull. Am. Astron. Soc.* **29**, 964.

BURBINE T. H., MEIBOM A. AND BINZEL R. P. (1996) Mantle material in the main belt: Battered to bits? *Meteorit. Planet. Sci.* **31**, 607–620.

BURBINE T. H., BINZEL R. P AND BUS S. J. (1998) Is Vesta the parent body of the "Vesta Chips"? Yes. (abstract). *Lunar Planet. Sci.* **29**, #1459, Lunar and Planetary Institute, Houston, Texas, USA (CD-ROM).

BURBINE T. H., MCCOY T. J., NITTLER L. R. AND BELL J. F., III (2001) Could 433 Eros have a primitive achondritic composition? (abstract). *Lunar Planet. Sci.* **32**, #1860, Lunar and Planetary Institute, Houston, Texas, USA (CD-ROM).

BUS S. J. (1999) Compositional structure in the asteroid belt: Results of a spectroscopic survey. Ph.D. thesis, Massachusetts Institute of Technology, Cambridge, Massachusetts, USA. 367 pp.

CLARK R. N. (1999) Spectroscopy of rocks and minerals and principles of spectroscopy. In *Remote Sensing for the Earth Sciences, Manual of Remore Sensing, Vol. 3* (eds. A. N. Rencz and R. A. Ryerson), pp. 3–58. John Wiley & Sons, Inc., New York, New York, USA.

CLARK R. N., SWAYZE G. A., GALLAGHER A. J., KING T. V. V. AND CALVIN W. M. (1993) *The U. S. Geological Survey, Digital Spectral Library: Version 1: 0.2 to 3.0 microns*. U.S. Geological Survey Open File Report 93-592. 1340 pp.

COCHRAN A. L. AND VILAS F. (1998) The changing spectrum of Vesta: Rotationally resolved spectroscopy of pyroxene on the surface. *Icarus* **134**, 207–212.

CONSOLMAGNO G. J. AND DRAKE M. J. (1977) Composition and evolution of the eucrite parent body: Evidence from rare earth elements. *Geochim. Cosmochim. Acta* **41**, 1271–1282.

CROWN D. A. AND PIETERS C. M. (1987) Spectral properties of plagioclase and pyroxene mixtures and the interpretation of lunar soil spectra. *Icarus* **72**, 492–506.

DESNOYERS C. AND JEROME D. Y. (1977) The Malvern howardite: A petrological and chemical discussion. *Geochim. Cosmochim. Acta* **41**, 81–86.

DODD R. T. (1981) *Meteorites, A Petrologic-Chemical Synthesis*. Cambridge University Press, Cambridge, U.K. 368 pp.

DRAKE M. J. (2001) Presidential Address: The eucrite/Vesta story. *Meteorit. Planet. Sci.* **36**, 501–513.

GAFFEY M. J. (1976) Spectral reflectance characteristics of the meteorite classes. *J. Geophys. Res.* **81**, 905–920.

GAFFEY M. J. (1984) Rotational spectral variations of asteroid (8) Flora: Implications for the nature of the S-type asteroids and for the parent bodies of the ordinary chondrites. *Icarus* **60**, 83–114.

GAFFEY M. J. (1997) Surface lithologic heterogeneity of asteroid 4 Vesta. *Icarus* **127**, 130–157.

GRADY M. M. (2000) *Catalogue of Meteorites*. Cambridge University Press, Cambridge, U.K. 689 pp.

GROSSMAN J. N. (1994) The Meteoritical Bulletin, No. 76, 1994 January: The U.S. Antarctic meteorite collection. *Meteoritics* **29**, 100–143.

GROVE T. L. AND BARTELS K. S. (1992) The relation between diogenite cumulates and eucrite magmas. *Proc. Lunar Planet. Sci. Conf.* **22nd**, 437–445.

HAZEN R. M., BELL P. M. AND MAO H. K. (1978) Effects of compositional variation on absorption spectra of lunar pyroxenes. *Proc. Lunar Sci. Conf.* **9th**, 2919–2934.

HINRICHS J. L., LUCEY P. G., ROBINSON M. S., MEIBOM A. AND KROT A. N. (1999) Implications of temperature-dependent near-IR spectral properties of common minerals and meteorites for remote sensing of asteroids. *Geophys. Res. Lett.* **26**, 1661–1664.

HIROI T. AND PIETERS C. M. (1998) Origin of Vestoids suggested from the space weathering trend in the visible reflectance spectra of HED meteorites and lunar soils. *Antarct. Met. Res.* **11**, 165–172.

HIROI T., MIYAMOTO M. AND TAKANO Y. (1985) An assignment of photon absorptions to Fe^{2+} and Cr^{3+} in pyroxenes and olivine by crystal field theory (abstract). *Lunar Planet. Sci.* **16**, 356–357.

HIROI T., PIETERS C. M. AND TAKEDA H. (1994) Grain size of the surface regolith of asteroid 4 Vesta estimated from its reflectance spectrum in comparison with HED meteorites. *Meteoritics* **29**, 394–396.

HIROI T., BINZEL R. P., SUNSHINE J. M., PIETERS C. M. AND TAKEDA H. (1995) Grain sizes and mineral compositions of surface regoliths of Vesta-like asteroids. *Icarus* **115**, 374–386.

JOHNSON T. V. AND FANALE F. P. (1973) Optical properties of carbonaceous chondrites and their relationship to asteroids. *J. Geophys. Res.* **78**, 8507–8518.

KITTS K. AND LODDERS K. (1998) Survey and evaluation of eucrite bulk compositions. *Meteorit. Planet. Sci.* **31 (Suppl.)**, A197–A213.

LANDOLT A. U. (1973) UBV photometric sequences in the celestial equatorial selected areas 92-115. *Astron. J.* **87**, 959–1020.

LARSON H. P. AND FINK U. (1975) Infrared spectral observations of asteroid 4 Vesta. *Icarus* **26**, 420–427.

LAZZARO D. *ET AL.* (2000) Discovery of a basaltic asteroid in the outer main belt. *Science* **288**, 2033–2035.

MARZARI F., CELLINO A., DAVIS D. R., FARINELLA P., ZAPPALÀ V. AND VANZANI V. (1996) Origin and evolution of the Vesta asteroid family. *Astron. Astrophys.* **316**, 248–262.

MASON B. (1962) *Meteorites*. John Wiley and Sons, Inc., New York, New York, USA. 274 pp.

MCCORD T. B., ADAMS J. B. AND JOHNSON T. V. (1970) Asteroid Vesta: Spectral reflectivity and compositional implications. *Science* **168**, 1445–1447.

MCCOY T. J., KEIL K., CLAYTON R. N., MAYEDA T. K., BOGARD D. D., GARRISON D. H. AND WIELER R. (1997) A petrologic and isotopic study of lodranites: Evidence for early formation as partial melt residues from heterogeneous precursors. *Geochim. Cosmochim. Acta* **61**, 623–637.

MCCOY T. J., NITTLER L. R., BURBINE T. H., TROMBKA J. I., CLARK P. E. AND MURPHY M. E. (2000) Anatomy of a partially differentiated asteroid: A "NEAR"-sighted view of acapulcoites and lodranites. *Icarus* **148**, 29–36.

MILANI A. AND KNEŽEVIĆ Z. (1994) Asteroid proper elements and the dynamical structure of the asteroid belt. *Icarus* **107**, 219–254.

MITTLEFEHLDT D. W. AND LINDSTROM M. M. (1991) Geochemistry of 5 Antarctic howardites and their clasts (abstract). *Lunar Planet. Sci.* **22**, 901–902.

MITTLEFEHLDT D. W., SEE T. H. AND HÖRZ F. (1992) Dissemination and fractionation of projectile materials in the impact melts from Wabar Crater, Saudi Arabia. *Meteoritics* **27**, 361–370.

MITTLEFEHLDT D. W., MCCOY T. J., GOODRICH C. A. AND KRACHER A. (1998) Non-chondritic meteorites from asteroidal bodies. In *Planetary Materials* (ed. J. J. Papike), pp. 4-1 to 4-195. Mineralogical Society of America, Washington, D.C., USA.

MIYAMOTO M. AND TAKEDA H. (1994) Evidence for excavation of deep crustal material of a Vesta-like body from Ca compositional gradients in pyroxene. *Earth Planet. Sci. Lett.* **122**, 343–349.

NOBLE S. K., PIETERS C. M., TAYLOR L. A., MORRIS R. V., ALLEN C. C., MCKAY D. S. AND KELLER L. P. (2001) The optical properties of the finest fraction of lunar soils: Implications for space weathering. *Meteorit. Planet. Sci.* **36**, 31–42.

OLSEN E. J., DOD B. D., SCHMITT R. A. AND SIPIERA P. P. (1987) Monticello: A glass-rich howardite. *Meteoritics* **22**, 81–96.

OLSEN E. J., FREDRIKSSON K., RAJAN S. AND NOONAN A. (1990) Chondrule-like objects and brown glasses in howardites. *Meteoritics* **25**, 187–194.

PIETERS C. M., FISCHER E. M., RODE O. AND BASU A. (1993) Optical effects of space weathering: The role of the finest fraction. *J. Geophys. Res.* **98**, 20 817–20 824.

PIETERS C. M., TAYLOR L. A., NOBLE S. K., KELLER L. P., HAPKE B., MORRIS R. V., ALLEN C. C., MCKAY D. S. AND WENTWORTH S. (2000) Space weathering on airless bodies: Resolving a mystery with lunar samples. *Meteorit. Planet. Sci.* **35**, 1101–1107.

REINSCH C. H. (1967) Smoothing by spline functions. *Numer. Math.* **10**, 177–183.

RUZICKA A., SNYDER G. A. AND TAYLOR L. A. (1997) Vesta as the howardite, eucrite and diogenite parent body: Implications for the size of a core and for large-scale differentiation. *Meteorit. Planet. Sci.* **32**, 825–840.

SCHWARZ C. AND MASON B. (1983) PCAA82502. *Antarctic Meteorite Newsletter* **6**, 12.

SCORE R. AND MASON B. (1986) ALH 85001. *Antarctic Meteorite Newsletter* **9**, 16.

TAKEDA H. AND GRAHAM A. L. (1991) Degree of equilibration of eucritic pyroxenes and thermal metamorphism of the earliest planetary crust. *Meteoritics* **26**, 129–134.

TAYLOR L. A., PIETERS C. M., KELLER L. P., MORRIS R. V., MCKAY D. S., PATCHEN A. AND WENTWORTH S. (2001) The effects of space weathering on Apollo 17 mare soils: Petrographic and chemical characterization. *Meteorit. Planet. Sci.* **36**, 285–299.

THOMAS P. C., BINZEL R. P., GAFFEY M. J., ZELLNER B. H., STORRS A. D. AND WELLS E. (1997a) Vesta: Spin pole, size, and shape from HST Images. *Icarus* **128**, 88–94.

THOMAS P. C., BINZEL R. P., GAFFEY M. J., STORRS A. D., WELLS E. N. AND ZELLNER B. H. (1997b) Impact excavation on asteroid 4 Vesta: Hubble Space Telescope results. *Science* **277**, 1492–1495.

VILAS F., COCHRAN A. L. AND JARVIS K. S. (2000) Vesta and the Vestoids: A new rock group? *Icarus* **147**, 119–128.

VOKROUHLICKÝ D. AND FARINELLA P. (2000) Efficient delivery of meteorites to the Earth from a wide range of asteroid parent bodies. *Nature* **407**, 606–608.

WASSON J. T. (1995) Sampling the asteroid belt: How biases make it difficult to establish meteorite-asteroid connections (abstract). *Meteoritics* **30**, 595.

WASSON J. T., CHAPMAN C. R., GROGAN K. AND DERMOTT S. F. (1996) Possible formation of the Vesta-like family asteroids and the main IRAS dust band by an oblique impact on Vesta (abstract). *Lunar Planet. Sci.* **27**, 1387–1388.

WASSON J. T., PIETERS C. M., FISENKO A. V., SEMJONOVA L. F., MOROZ L. V. AND WARREN P. H. (1997) Simulation of space weathering of HED meteorites by laser impulse irradiation (abstract). *Lunar Planet. Sci.* **28**, 1505–1506.

WELTEN K. C., LINDNER L., VAN DER BORG K., LOEKEN T., SCHERER P. AND SCHULTZ L. (1997) Cosmic-ray exposure ages of diogenites and the recent collisional history of the howardite, eucrite and diogenite parent body/bodies. *Meteorit. Planet. Sci.* **32**, 891–902.

WILLIAMS J. G. (1979) Proper elements and family memberships of the asteroids. In *Asteroids* (ed. T. Gehrels), pp. 1040–1063. Univ. Arizona Press, Tucson, Arizona, USA.

XU S., BINZEL R. P., BURBINE T. H. AND BUS S. J. (1995) Small main-belt asteroid spectroscopic survey: Initial results. *Icarus* **115**, 1–35.

YAMADA M., SASAKI S., NAGAHARA H., FUJIWARA A., HASEGAWA S., YANO H., HIROI T., OHASHI H. AND OTAKE H. (1999) Simulation of space weathering of planet-forming materials: Nanosecond pulse laser irradiation and proton implantation on olivine and pyroxene samples. *Earth Planets Space* **51**, 1255–1265.

YAMAGUCHI A., MORI H. AND TAKEDA H. (1993) Mineralogy and shock textures in the Padvarninkai eucrite (abstract). *Meteoritics* **28**, 462–463.

ZAPPALÀ V., CELLINO A., FARINELLA P. AND KNEŽEVIĆ Z. (1990) Asteroid families I. Identification by hierarchical clustering and reliability assessment. *Astron. J.* **100**, 2030–2046.

ZAPPALÀ V., BENDJOYA PH., CELLINO A., FARINELLA P. AND FROESCHLÉ C. (1995) Asteroid families: Search of a 12,487-asteroid sample using two different clustering techniques. *Icarus* **116**, 291–314.